The Astrophysical Journal Supplement Series, 148:175–194, 2003 September

FIRST-YEAR *WILKINSON MICROWAVE ANISOTROPY PROBE* (*WMAP*)[1] OBSERVATIONS: DETERMINATION OF COSMOLOGICAL PARAMETERS

D. N. Spergel,[2] L. Verde,[2,3] H. V. Peiris,[2] E. Komatsu,[2] M. R. Nolta,[4] C. L. Bennett,[5] M. Halpern,[6] G. Hinshaw,[5] N. Jarosik,[4] A. Kogut,[5] M. Limon,[5,7] S. S. Meyer,[8] L. Page,[4] G. S. Tucker,[5,7,9] J. L. Weiland,[10] E. Wollack,[5] and E. L. Wright[11]

Received 2003 February 11; accepted 2003 May 20

ABSTRACT

WMAP precision data enable accurate testing of cosmological models. We find that the emerging standard model of cosmology, a flat Λ-dominated universe seeded by a nearly scale-invariant adiabatic Gaussian fluctuations, fits the *WMAP* data. For the *WMAP* data only, the best-fit parameters are $h = 0.72 \pm 0.05$, $\Omega_b h^2 = 0.024 \pm 0.001$, $\Omega_m h^2 = 0.14 \pm 0.02$, $\tau = 0.166^{+0.076}_{-0.071}$, $n_s = 0.99 \pm 0.04$, and $\sigma_8 = 0.9 \pm 0.1$. With parameters fixed only by *WMAP* data, we can fit finer scale cosmic microwave background (CMB) measurements and measurements of large-scale structure (galaxy surveys and the Lyα forest). This simple model is also consistent with a host of other astronomical measurements: its inferred age of the universe is consistent with stellar ages, the baryon/photon ratio is consistent with measurements of the [D/H] ratio, and the inferred Hubble constant is consistent with local observations of the expansion rate. We then fit the model parameters to a combination of *WMAP* data with other finer scale CMB experiments (ACBAR and CBI), 2dFGRS measurements, and Lyα forest data to find the model's best-fit cosmological parameters: $h = 0.71^{+0.04}_{-0.03}$, $\Omega_b h^2 = 0.0224 \pm 0.0009$, $\Omega_m h^2 = 0.135^{+0.008}_{-0.009}$, $\tau = 0.17 \pm 0.06$, $n_s(0.05\ \mathrm{Mpc}^{-1}) = 0.93 \pm 0.03$, and $\sigma_8 = 0.84 \pm 0.04$. *WMAP*'s best determination of $\tau = 0.17 \pm 0.04$ arises directly from the temperature-polarization (TE) data and not from this model fit, but they are consistent. These parameters imply that the age of the universe is 13.7 ± 0.2 Gyr. With the Lyα forest data, the model favors but does not require a slowly varying spectral index. The significance of this running index is sensitive to the uncertainties in the Lyα forest.

By combining *WMAP* data with other astronomical data, we constrain the geometry of the universe, $\Omega_{\mathrm{tot}} = 1.02 \pm 0.02$, and the equation of state of the dark energy, $w < -0.78$ (95% confidence limit assuming $w \geq -1$). The combination of *WMAP* and 2dFGRS data constrains the energy density in stable neutrinos: $\Omega_\nu h^2 < 0.0072$ (95% confidence limit). For three degenerate neutrino species, this limit implies that their mass is less than 0.23 eV (95% confidence limit). The *WMAP* detection of early reionization rules out warm dark matter.

Subject headings: cosmic microwave background — cosmological parameters — cosmology: observations — early universe

On-line material: color figure

1. INTRODUCTION

Over the past century, a standard cosmological model has emerged: with relatively few parameters, the model describes the evolution of the universe and astronomical observations on scales ranging from a few to thousands of megaparsecs. In this model the universe is spatially flat, homogeneous, and isotropic on large scales, composed of radiation, ordinary matter (electrons, protons, neutrons, and neutrinos), nonbaryonic cold dark matter, and dark energy. Galaxies and large-scale structure grew gravitationally from tiny, nearly scale-invariant adiabatic Gaussian fluctuations. The *Wilkinson Microwave Anisotropy Probe* (*WMAP*) data offer a demanding quantitative test of this model.

The *WMAP* data are powerful because they result from a mission that was carefully designed to limit systematic measurement errors (Bennett et al. 2003a, 2003b; Hinshaw et al. 2003b). A critical element of this design includes differential measurements of the full sky with a complex sky scan pattern. The nearly uncorrelated noise between pairs of pixels, the accurate in-flight determination of the beam patterns (Page et al. 2003a, 2003c; Barnes et al. 2003), and the well-understood properties of the radiometers (Jarosik et al. 2003a, 2003b) are invaluable for this analysis.

Our basic approach in this analysis is to begin by identifying the simplest model that fits the *WMAP* data and determining the best-fit parameters for this model using *WMAP* data only without the use of any significant priors on parameter values. We then compare the predictions of this model to other data sets and find that the model is

[1] *WMAP* is the result of a partnership between Princeton University and the NASA Goddard Space Flight Center. Scientific guidance is provided by the *WMAP* Science Team.

[2] Department of Astrophysical Sciences, Princeton University, Princeton, NJ 08544.

[3] *Chandra* Postdoctral Fellow.

[4] Department of Physics, Jadwin Hall, Princeton, NJ 08544.

[5] NASA Goddard Space Flight Center, Code 685, Greenbelt, MD 20771.

[6] Department of Physics and Astronomy, University of British Columbia, Vancouver, BC V6T 1Z1, Canada.

[7] National Research Council (NRC) Fellow.

[8] Departments of Astrophysics and Physics, EFI, and CfCP, University of Chicago, Chicago, IL 60637.

[9] Department of Physics, Brown University, Providence, RI 02912.

[10] Science Systems and Applications, Inc. (SSAI), 10210 Greenbelt Road, Suite 600, Lanham, MD 20706.

[11] Department of Astronomy, UCLA, P.O. Box 951562, Los Angeles, CA 90095-1562.

basically consistent with these data sets. We then fit to combinations of the *WMAP* data and other astronomical data sets and find the best-fit global model. Finally, we place constraints on alternatives to this model.

We begin by outlining our methodology (§ 2). Verde et al. (2003) describe the details of the approach used here to compare theoretical predictions of cosmological models to data. In § 3, we fit a simple, six-parameter ΛCDM model to the *WMAP* data set (temperature-temperature and temperature-polarization angular power spectra). In § 4 we show that this simple model provides an acceptable fit not only to the *WMAP* data, but also to a host of astronomical data. We use the comparison with these other data sets to test the validity of the model rather than further constrain the model parameters. In § 5, we include large-scale structure data from the Anglo-Australian Telescope Two-Degree Field Galaxy Redshift Survey (2dFGRS; Colless et al. 2001) and Lyα forest data to perform a joint likelihood analysis for the cosmological parameters. We find that the data favor a slowly varying spectral index. This seven-parameter model is our best fit to the full data set. In § 6, we relax some of the minimal assumptions of the model by adding extra parameters to the model. We examine nonflat models, dark energy models in which the properties of the dark energy are parameterized by an effective equation of state, and models with gravity waves. By adding extra parameters we introduce degenerate sets of models consistent with the *WMAP* data alone. We lift these degeneracies by including additional microwave background data sets (Cosmic Background Imager [CBI], Arcminute Cosmology Bolometer Array Receiver [ACBAR]) and observations of large-scale structure. We use these combined data sets to place strong limits on the geometry of the universe, the neutrino mass, the energy density in gravity waves, and the properties of the dark energy. In § 7, we note an intriguing discrepancy between the standard model and the *WMAP* data on the largest angular scales and speculate on its origin. In § 8, we conclude and present parameters for our best-fit model.

2. BAYESIAN ANALYSIS OF COSMOLOGICAL DATA

The basic approach of this paper is to find the simplest model consistent with cosmological data. We begin by fitting a simple six-parameter model first to the *WMAP* data and then to other cosmological data sets. We then consider more complex cosmological models and evaluate whether they are a better description of the cosmological data. Since Komatsu et al. (2003) found no evidence for non-Gaussianity in the *WMAP* data, we assume the primordial fluctuations are Gaussian random phase throughout this paper. For each model studied in the paper, we use a Monte Carlo Markov chain to explore the likelihood surface. We assume flat priors in our basic parameters and impose positivity constraints on the matter and baryon density (these limits lie at such low likelihood that they are unimportant for the models). We assume a flat prior in τ, the optical depth, but bound $\tau < 0.3$. This prior has little effect on the fits but keeps the Markov chain out of unphysical regions of parameter space. For each model, we determine the best-fit parameters from the peak of the N-dimensional likelihood surface. For each parameter in the model we also compute its one dimensional likelihood function by marginalizing over all other parameters; we then quote the (one-dimensional) expectation value[12] as our best estimate for the parameter:

$$\langle \alpha_i \rangle = \int d^N \alpha \mathscr{L}(\boldsymbol{\alpha}) \alpha_i \, , \tag{1}$$

where $\boldsymbol{\alpha}$ denotes a point in the N-dimensional parameter space (in our application these are points—sets of cosmological parameters—in the output of the Markov chain), $\mathscr{L}$ denotes the likelihood (in our application the "weight" given by the chain to each point). The *WMAP* temperature (TT) angular power spectrum and the *WMAP* temperature-polarization (TE) angular power spectrum are our core data sets for the likelihood analysis. Hinshaw et al. (2003b) and Kogut et al. (2003) describe how to obtain the temperature and temperature-polarization angular power spectra respectively from the maps. Verde et al. (2003) describe our basic methodology for evaluating the likelihood functions using a Monte Carlo Markov chain algorithm and for including data sets other than *WMAP* in our analysis. In addition to *WMAP* data we use recent results from the CBI (Pearson et al. 2002) and ACBAR (Kuo et al. 2002) experiments. We also use the 2dFGRS measurements of the power spectrum (Percival et al. 2001) and the bias parameter (Verde et al. 2002), measurements of the Lyα power spectrum (Croft et al. 2002; Gnedin & Hamilton 2002), Type Ia supernova measurements of the angular diameter distance relation (Garnavich et al. 1998; Riess et al. 2001), and the *Hubble Space Telescope* (*HST*) Key Project measurements of the local expansion rate of the universe (Freedman et al. 2001).

3. POWER-LAW ΛCDM MODEL AND THE *WMAP* DATA

We begin by considering a basic cosmological model: a flat universe with radiation, baryons, cold dark matter and cosmological constant, and a power-law power spectrum of adiabatic primordial fluctuations. As we will see, this model does a remarkably good job of describing *WMAP* TT and TE power spectra with only six parameters: the Hubble constant h (in units of 100 km s^{-1} Mpc^{-1}), the physical matter and baryon densities $w_m \equiv \Omega_m h^2$ and $w_b \equiv \Omega_b h^2$, the optical depth to the decoupling surface, τ, the scalar spectral index n_s, and A, the normalization parameter in the CMBFAST code version 4.1 with option UNNORM. Verde et al. (2003) discuss the relationship between A and the amplitude of curvature fluctuations at horizon crossing, $|\Delta R|^2 = 2.95 \times 10^{-9} A$. In § 4, we show that this model is also in acceptable agreement with a wide range of astronomical data.

This simple model provides an acceptable fit to both the *WMAP* TT and TE data (see Figs. 1 and 2). The reduced[13] $\chi^2_{\rm eff}$ for the full fit is 1.066 for 1342 degrees of freedom, which has a probability of ~5%. For the TT data alone,

[12] In a Monte Carlo Markov chain, it is a more robust quantity than the mode of the a posteriori marginalized distribution.

[13] Here, $\chi^2_{\rm eff} \equiv -2 \ln \mathscr{L}$ and ν is number of data minus the number of parameters. We have used 100,000 Monte Carlo realizations of the *WMAP* data with our mask-, noise-, and angle-averaged beams and found that the $\langle -2 \ln \mathscr{L}/\nu \rangle = 1$ for the simulated temperature data.

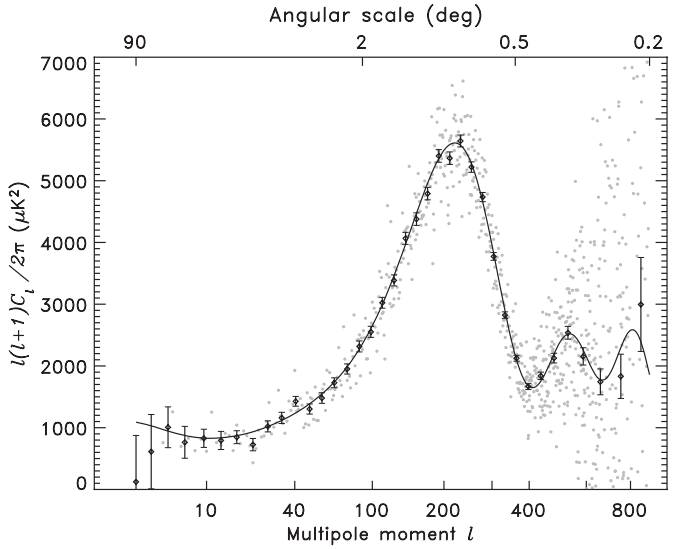

FIG. 1.—Comparison of the best-fit power-law ΛCDM model to the *WMAP* temperature angular power spectrum. The gray dots are the unbinned data. [*See the electronic edition of the Journal for a color version of this figure.*]

$\chi^2_{\rm eff}/\nu = 1.09$, which for 893 degrees of freedom has a probability of 3%. Most of the excess $\chi^2_{\rm eff}$ is due to the inability of the model to fit sharp features in the power spectrum near $\ell \sim 120$, the first TT peak and at $\ell \sim 350$. In Figure 3 we show the contribution to $\chi^2_{\rm eff}$ per multipole. The overall excess variance is likely due to our not including several effects, each contributing roughly 0.5%–1% to our power spectrum covariance near the first peak and trough: gravitational lensing of the CMB (Hu 2001), the spatial variations in the effective beam of the *WMAP* experiment due to variations in our scan orientation between the ecliptic pole and plane regions (Page et al. 2003a; Hinshaw et al. 2003a), and non-Gaussianity in the noise maps due to the $1/f$ striping. Including these effects would increase our estimate of the power spectrum uncertainties and improve our estimate of $\chi^2_{\rm eff}$. Our next data release will include the corrections and errors associated with the beam asymmetries. The features in the measured power spectrum could be due to underlying features in the primordial power spectrum (see § 5 of Peiris et al. 2003), but we do not yet attach cosmological significance to them.

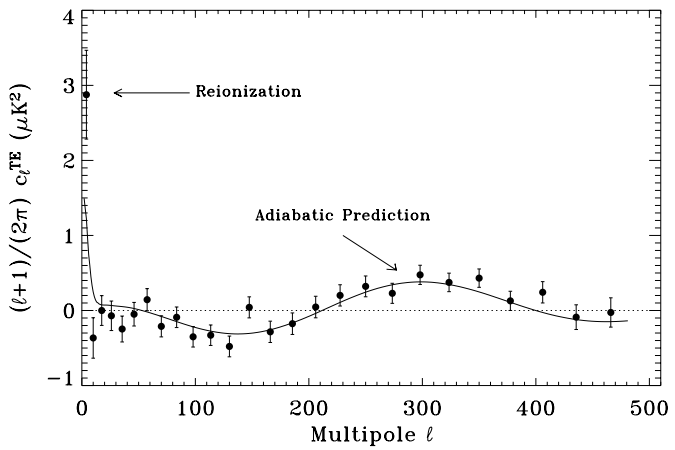

FIG. 2.—Comparison of the best-fit power-law ΛCDM model to the *WMAP* temperature angular power spectrum.

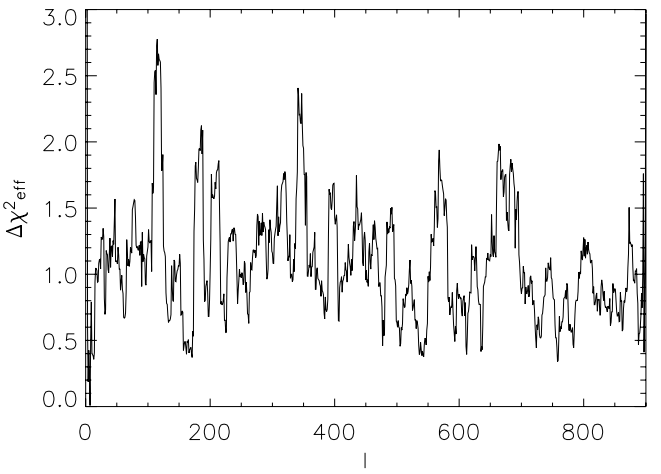

FIG. 3.—Contribution to $2\ln\mathcal{L}$ per multipole binned at $\Delta\ell = 15$. The excess χ^2 comes primarily from three regions, one around $\ell \sim 120$, one around $\ell \sim 200$, and the other around $\ell \sim 340$.

Table 1 lists the best-fit parameters using the *WMAP* data alone for this model and Figure 4 shows the marginalized probabilities for each of the basic parameters in the model. The values in the second column of Table 1 (and the subsequent parameter tables) are expectation values for the marginalized distribution of each parameter, and the errors are the 68% confidence interval. The values in the third column are the values at the peak of the likelihood function. Since we are projecting a high dimensional likelihood function, the peak of the likelihood is not the same as the expectation value of a parameter. Most of the basic parameters are remarkably well determined within the context of this model. Our most significant parameter degeneracy (see Fig. 5) is a degeneracy between n_s and τ. The TE data favors $\tau \sim 0.17$ (Kogut et al. 2003); on the other hand, the low value of the quadrupole (see Fig. 1 and § 7) and the relatively low amplitude of fluctuations for $\ell < 10$ disfavor high τ as reionization produces additional large-scale anisotropies. Because of the combination of these two effects, the likelihood surface is quite flat at its peak: the likelihood changes by only 0.05 as τ changes from 0.11 to 0.19. This particular shape depends upon the assumed form of the power spectrum: in § 5.2, we show that models with a scale-dependent spectral index have a narrower likelihood function that is more centered around $\tau = 0.17$.

TABLE 1

POWER-LAW ΛCDM MODEL PARAMETERS: *WMAP* DATA ONLY

Parameter	Mean (68% Confidence Range)	Maximum Likelihood
Baryon density, $\Omega_b h^2$.....	0.024 ± 0.001	0.023
Matter density, $\Omega_m h^2$.....	0.14 ± 0.02	0.13
Hubble constant, h.....	0.72 ± 0.05	0.68
Amplitude, A	0.9 ± 0.1	0.78
Optical depth, τ.....	$0.166^{+0.076}_{-0.071}$	0.10
Spectral index, n_s.....	0.99 ± 0.04	0.97
$\chi^2_{\rm eff}/\nu$		1431/1342

NOTE.—Fit to *WMAP* data only.

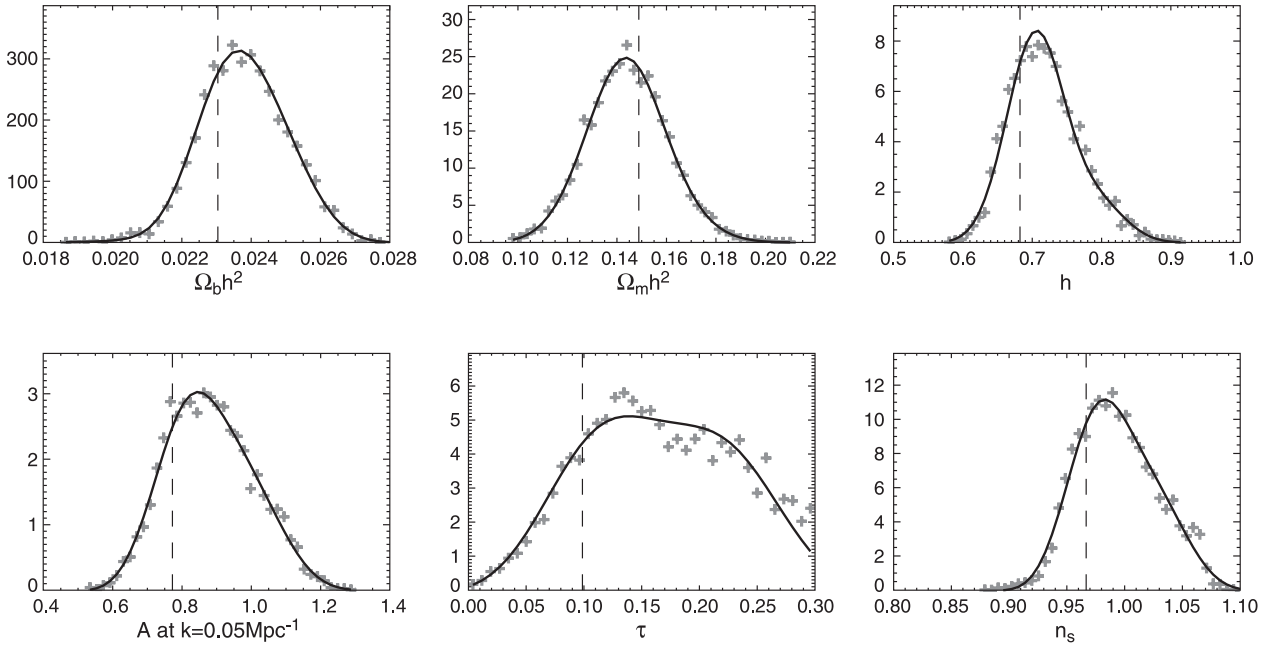

FIG. 4.—Likelihood function of the *WMAP* TT+TE data as a function of the basic parameters in the power-law ΛCDM *WMAP* model ($\Omega_b h^2$, $\Omega_m h^2$, h, A, n_s and τ.) The points are the binned marginalized likelihood from the Markov chain, and the solid curve is an Edgeworth expansion of the Markov chain's points. The marginalized likelihood function is nearly Gaussian for all of the parameters except for τ. The dashed lines show the maximum-likelihood values of the global six-dimensional fit. Since the peak in the likelihood, $x_{\rm ML}$, is not the same as the expectation value of the likelihood function, $\langle x \rangle$, the dashed line does not lie at the center of the projected likelihood.

Since the *WMAP* data allows us to accurately determine many of the basic cosmological parameters, we can now infer a number of important derived quantities to very high accuracy; we do this by computing these quantities for each model in the Monte Carlo Markov chain and use the chain to determine their expectation values and uncertainties.

Table 2 lists cosmological parameters based on fitting a power-law (PL) CDM model to the *WMAP* data only. The parameters $t_{\rm dec}$ and $z_{\rm dec}$ are determined by using the CMBFAST code (Seljak & Zaldarriaga 1996) to compute the redshift of the CMB "photosphere" (the peak in the photon visibility function). We determine the thickness of the decoupling surface by measuring $\Delta z_{\rm dec}$ and $\Delta t_{\rm dec}$, the full width at half-maximum of the visibility function. The age of the universe is derived by integrating the Friedmann equation, and σ_8 (the linear theory predictions for the amplitude of fluctuations within 8 Mpc h^{-1} spheres) from the linear matter power spectrum at $z = 0$ is computed by CMBFAST.

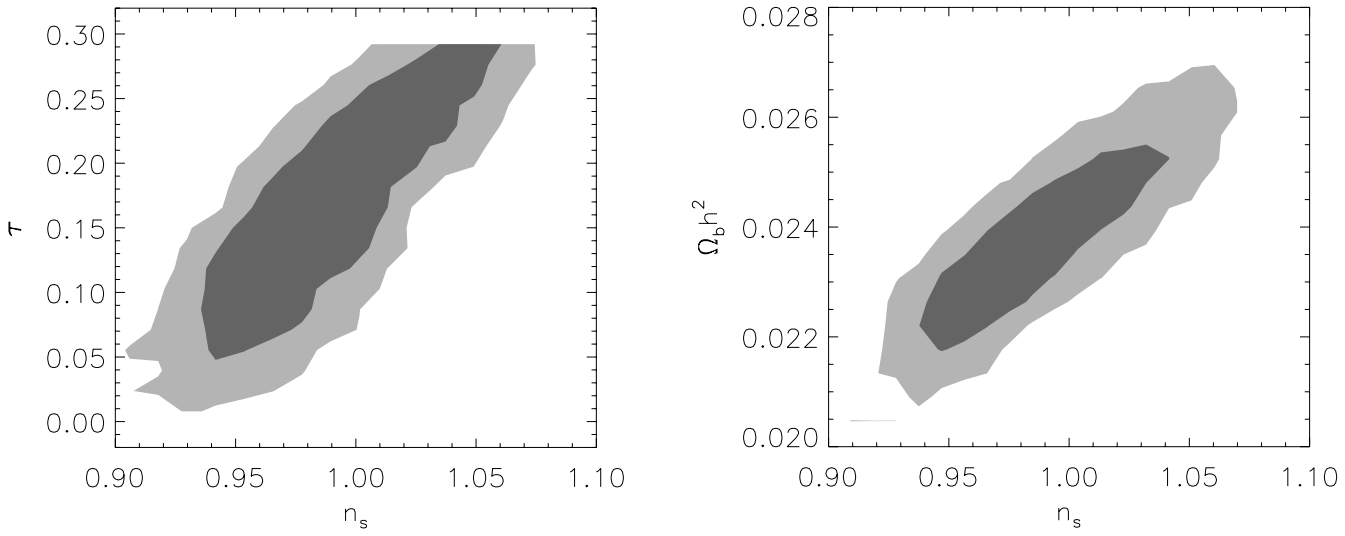

FIG. 5.—Spectral index constraints. *Left*: n_s-τ degeneracy in the *WMAP* data for a power-law ΛCDM model. The TE observations constrain the value of τ and the shape of the $C_l^{\rm TT}$ spectrum constrain a combination of n_s and τ. *Right*: n_s-$\Omega_b h^2$ degeneracy. The shaded regions show the joint 1 and 2 σ confidence regions.

TABLE 2
Derived Cosmological Parameters

Parameter	Mean (68% Confidence Range)
Amplitude of galaxy fluctuations, σ_8	0.9 ± 0.1
Characteristic amplitude of velocity fluctuations, $\sigma_8\Omega_m^{0.6}$	0.44 ± 0.10
Baryon density/critical density, Ω_b	0.047 ± 0.006
Matter density/critical density, Ω_m	0.29 ± 0.07
Age of the universe, t_0	13.4 ± 0.3 Gyr
Redshift of reionization,[a] z_r	17 ± 5
Redshift at decoupling, $z_{\rm dec}$	1088^{+1}_{-2}
Age of the universe at decoupling, $t_{\rm dec}$	372 ± 14 kyr
Thickness of surface of last scatter, $\Delta z_{\rm dec}$	194 ± 2
Thickness of surface of last scatter, $\Delta t_{\rm dec}$	115 ± 5 kyr
Redshift at matter/radiation equality, $z_{\rm eq}$	3454^{+385}_{-392}
Sound horizon at decoupling, r_s	144 ± 4 Mpc
Angular diameter distance to the decoupling surface, d_A	13.7 ± 0.5 Gpc
Acoustic angular scale,[b] ℓ_A	299 ± 2
Current density of baryons, n_b	$(2.7 \pm 0.1) \times 10^{-7}$ cm^{-3}
Baryon/photon ratio, η	$(6.5^{+0.4}_{-0.3}) \times 10^{-10}$

Note.—Fit to the *WMAP* data only.
[a] Assumes ionization fraction, $x_e = 1$.
[b] $l_A = \pi d_C / r_s$.

4. COMPARSION WITH ASTRONOMICAL PREDICTIONS

In this section, we compare the predictions of the best-fit power-law ΛCDM model to other cosmological observations. We also list in Table 10 the best-fit model to the full data set: a ΛCDM model with a running spectral index (see § 5.2). In particular, we consider determinations of the local expansion rate (i.e., the Hubble constant), the amplitude of fluctuations on galaxy scales, the baryon abundance, ages of the oldest stars, large-scale structure data, and Type Ia supernova data. We also consider whether our determination of the reionization redshift is consistent with the prediction for structure formation in our best-fit universe and with recent models of reionization. In §§ 5 and 6, we add some of these data sets to the *WMAP* data to better constrain parameters and cosmological models.

4.1. *Hubble Constant*

CMB observations do not directly measure the local expansion rate of the universe rather they measure the conformal distance to the decoupling surface and the matter-radiation ratio through the amplitude of the early integrated Sachs-Wolfe (ISW) contribution relative to the height of the first peak. For our power-law ΛCDM model, this is enough information to "predict" the local expansion rate. Thus, local Hubble constant measurements are an important test of our basic model.

The *HST* Key Project (Freedman et al. 2001) has carried out an extensive program of using Cepheids to calibrate several different secondary distance indicators (Type Ia supernovae, Tully-Fisher, Type II supernovae, and surface brightness fluctuations). With a distance modulus of 18.5 for the LMC, their combined estimate for the Hubble constant is $H_0 = 72 \pm 3(\text{stat.}) \pm 7(\text{syst.})$ km s^{-1} Mpc^{-1}. The agreement between the *HST* Key Project value and our value, $h = 0.72 \pm 0.05$, is striking, given that the two methods rely on different observables, different underlying physics, and different model assumptions.

As we will show in § 6, models with equation of state for the dark energy very different from a cosmological constant (i.e., $w = -1$) fit the *WMAP* data only if the Hubble constant is much smaller than the *HST* Key Project value. An independent determination of the Hubble constant that makes different assumptions than the traditional distance ladder can be obtained by combining Sunyaev-Zel'dovich and X-ray flux measurements of clusters of galaxies, under the assumption of sphericity for the density and temperature profile of clusters. This method is sensitive to the Hubble constant at intermediate redshifts ($z \sim 0.5$), rather than in the nearby universe. Reese et al. (2002), Jones et al. (2001), and Mason et al. (2001) have obtained values for the Hubble constant systematically smaller than the *HST* Key Project and *WMAP* ΛCDM model determinations, but all consistent at the $1\,\sigma$ level. Table 3 summarizes recent Hubble constant determinations and compares them with the *WMAP* ΛCDM model value.

4.2. *Amplitude of Fluctuations*

The overall amplitude of fluctuations on large-scale structure scales has been recently determined from weak lensing surveys, clusters number counts, and peculiar velocities from galaxy surveys. Weak-lensing surveys and peculiar velocity measurements are most sensitive to the combination $\sigma_8\Omega_m^{0.6}$, cluster abundance at low redshift is sensitive to

TABLE 3
Recent Hubble Constant Determinations

Method	Mean (68% Confidence Range)	Reference
HST Key Project	$72 \pm 3 \pm 7$	1
Sunyaev-Zel'dovich+X-ray	$60 \pm 4^{+13}_{-18}$	2
	$66^{+14}_{-11} \pm 15$	3
WMAP PL ΛCDM model	72 ± 5	§ 3

References.—(1) Freedman et al. (2001); (2) Reese et al. (2002); (3) Reese et al. (2002).

TABLE 4
AMPLITUDE OF FLUCTUATIONS, σ_8

Method	Mean (68% Confidence Range)	Reference
PL ΛCDM+*WMAP*	0.9 ± 0.1	§ 3
Weak lensing[a,b]	0.72 ± 0.18	1
	$0.86^{+0.10}_{-0.09}$	2
	$0.69^{+0.12}_{-0.16}$	3
	0.96 ± 0.12	4
	0.92 ± 0.2	5
	0.98 ± 0.12	6
Galaxy velocity fields[b]	0.73 ± 0.1	7
CBI SZ detection	1.04 ± 0.12[c]	8
High-redshift clusters[b]	0.95 ± 0.1	9

[a] Since most weak lensing papers report 95% confidence limits in their papers, the table lists the 95% confidence limit for these experiments.

[b] All of the σ_8 measurements have been normalized to $\Omega_m = 0.287$, the best-fit value for a fit to the *WMAP* data only.

[c] 95% confidence limit.

REFERENCES.—(1) Brown et al. 2002; (2) Hoekstra et al. 2002; (3) Jarvis et al. 2002; (4) Bacon et al. 2002; (5) Refregier et al. 2002; (6) Van Waerbeke et al. 2002a; (7) Willick & Strauss 1998; (8) Komatsu & Seljak 2002; (9) Bahcall & Bode 2002.

a very similar parameter combination $\sigma_8\Omega_m^{0.5}$, but counts of high-redshift clusters can break the degeneracy.

4.2.1. *Weak Lensing*

Weak lensing directly probes the amplitude of mass fluctuations along the line of sight to the background galaxies. Once the redshift distribution of the background galaxies is known, this technique directly probes gravitational potential fluctuations and therefore can be easily compared with our CMB model predictions for the amplitude of dark matter fluctuations. Several groups have reported weak shear measurements within the past year (see Table 4 and Van Waerbeke et al. 2002b for recent review): while there is significant scatter in the reported amplitude, the best-fit model to the *WMAP* data lies in the middle of the reported range. As these shear measurements continue to improve, the combination of *WMAP* observations and lensing measurements will be a powerful probe of cosmological models.

4.2.2. *Galaxy Velocity Fields*

The galaxy velocity fields are another important probe of the large-scale distribution of matter. The Willick & Strauss (1998) analysis of the Mark III velocity fields and the *IRAS* redshift survey yields $\beta^{\rm IRAS} = 0.50 \pm 0.04$. *IRAS* galaxies are less clustered than optically selected galaxies; Fisher et al. (1994) find $\sigma_8^{\rm IRAS} = 0.69 \pm 0.04$, implying $\sigma_8^{\rm mass}\Omega_m^{0.6} = 0.345 \pm 0.05$, consistent with our ΛCDM model value of 0.44 ± 0.10.

4.2.3. *Cluster Number Counts*

Our best fit to the *WMAP* data is $\sigma_8\Omega_m^{0.5} = 0.48 \pm 0.12$. The Bahcall et al. (2002b) recent study of the mass function of 300 clusters at redshifts $0.1 < z < 0.2$ in the early Sloan Digital Sky Survey data release yields $\sigma_8\Omega_m^{0.6} = 0.33 \pm 0.03$. This difference may reflect the sensitivity of the cluster measurements to the conversion of cluster richness to mass. Observations of the mass function of high-redshift clusters break the degeneracy between σ_8 and Ω_m. The recent Bahcall & Bode (2002) analysis of the abundance of massive clusters at $z = 0.5$–0.8 yields $\sigma_8 = 0.95 \pm 0.1$ for $\Omega_m = 0.25$. Other cluster analysis yield different values: the Borgani et al. (2001) best-fit values for a large sample of X-ray clusters are $\sigma_8 = 0.66^{+0.05}_{-0.05}$ and $\Omega_m = 0.35^{+0.13}_{-0.10}$. On the other hand, Reiprich & Böhringer (2002) find very different values: $\sigma_8 = 0.96^{+0.15}_{-0.12}$ and $\Omega_m = 0.12^{+0.06}_{-0.04}$. Pierpaoli et al. (2002) discuss the wide range of values that different X-ray analyses find for σ_8. With the larger REFLEX sample, Schuecker et al. (2003a) find $\sigma_8 = 0.711^{+0.039}_{-0.031}(\text{stat.})^{+0.120}_{-0.162}(\text{syst.})$ and $\Omega_m = 0.341^{+0.031}_{-0.029}(\text{stat.})^{+0.087}_{-0.071}(\text{syst.})$ The best-fit *WMAP* values lie in the middle of the relevant range.

Measurements of the contribution to the CMB power spectrum on small scales from the Sunyaev-Zel'dovich effect also probe the number density of high-redshift clusters. The recent CBI detection of excess fluctuations (Mason et al. 2001; Bond et al. 2002) at $\ell > 1500$ implies $\sigma_8 = 1.04 \pm 0.12$ (Komatsu & Seljak 2002), if the signal is due to the Sunyaev-Zel'dovich effect.

4.3. *Baryon Abundance*

Both the amplitude of the acoustic peaks in the CMB spectrum (Bond & Efstathiou 1984) and the primordial abundance of deuterium (Boesgaard & Steigman 1985) are sensitive functions of the cosmological baryon density. Since the height and position of the acoustic peaks depend upon the properties of the cosmic plasma 372,000 years after the big bang and the deuterium abundance depend on physics only 3 minutes after the big bang, comparing the baryon density constraints inferred from these two different probes provides an important test of the big bang model. The best-fit baryon abundance based on *WMAP* data only for the PL ΛCDM model, $\Omega_b h^2 = 0.0237^{+0.0013}_{-0.0012}$, implies a baryon/photon ratio of $\eta = (6.5^{+0.4}_{-0.3}) \times 10^{-10}$. For this abundance, standard big bang nucleosynthesis (Burles et al. 2001) implies a primordial deuterium abundance relative to hydrogen: $[\text{D/H}] = 2.37^{+0.19}_{-0.21} \times 10^{-5}$. As will be clear from §§ 5 and 6, the best-fit $\Omega_b h^2$ value for our fits is relatively insensitive to cosmological model and data set combination as it depends primarily on the ratio of the first to second peak heights (Page et al. 2003b). For the running spectral index model discussed in § 5.2, the best-fit baryon abundance, $\Omega_b h^2 = 0.0224 \pm 0.0009$, implies a primordial $[\text{D/H}] = 2.62^{+0.18}_{-0.20} \times 10^{-5}$ (see Table 5).

How does the primordial deuterium abundance inferred from CMB compare with that observed from the ISM? Galactic chemical evolution destroys deuterium because the deuterium nucleus is relatively fragile and is easily destroyed in stars. Thus, measurements of the deuterium abundance

TABLE 5
MEASURED RATIO OF DEUTERIUM TO HYDROGEN

Quasar	[D/H]	Reference
Q0130−403	$< 6.8 \times 10^{-5}$	1
PKS 1937−1009	$3.25 \pm 0.3 \times 10^{-5}$	2
Q1009+299	$4.0 \pm 0.65 \times 10^{-5}$	3
HS 0105+1619	$2.5 \pm 0.25 \times 10^{-5}$	4
Q2206−199	$1.65 \pm 0.35 \times 10^{-5}$	5
Q0347−383	$3.75 \pm 0.25 \times 10^{-5}$	6
Q1234+3047	$2.42^{+0.35}_{-0.25} \times 10^{-5}$	7

REFERENCES.—(1) Kirkman et al. 2000; (2) Burles & Tytler 1998a; (3) Burles & Tytler 1998b; (4) O'Meara et al. 2001; (5) Pettini & Bowen 2001; (6) Levshakov et al. 2003; (7) Kirkman et al. 2003.

within the Galaxy are usually treated as lower limits on the primordial abundance (Epstein et al. 1976). Local measurements of D and H absorption find [D/H] abundance near 1.5×10^{-5}, while more distant measurements by *IMAP* and *FUSE* find significant variation in deuterium abundances suggesting a complex Galactic chemical history (Jenkins et al. 1999; Sonneborn et al. 2000; Moos et al. 2002).

Observations of Lyα clouds reduce the need to correct the deuterium abundance for stellar processing as these systems have low (but nonzero) metal abundances. These observations require identifying gas systems that do not have serious interference from the Lyα forest. The Kirkman et al. (2003) analysis of QSO HS 243+3057 yields a D/H ratio of $2.42^{+0.35}_{-0.25} \times 10^{-5}$. They combine this measurement with four other D/H measurements (Q0130−4021: D/H $< 6.8 \times 10^{-5}$; Q1009+2956: $3.98 \pm 0.70 \times 10^{-5}$; PKS 1937−1009: $3.25 \pm 0.28 \times 10^{-5}$; and QSO HS 0105+1619: $2.5 \pm 0.25 \times 10^{-5}$) to obtain their current best D/H ratio: $2.78^{+0.44}_{-0.38} \times 10^{-5}$, implying $\Omega_b h^2 = 0.0214 \pm 0.0020$. D'Odorico et al. (2001) find $2.24 \pm 0.67 \times 10^{-5}$ from their observations of Q0347−3819 (although a reanalysis of the system by Levshakov et al. 2003 find a higher D/H value: 3.75 ± 0.25). Pettini & Bowen (2001) report a D/H abundance of $1.65 \pm 0.35 \times 10^{-5}$ from STIS measurements of QSO 2206−199, a low-metallicity ($Z \sim 1/200$) damped Lyα system (DLA). The *WMAP* value lies between the Pettini & Bowen (2001) estimate from DLAs, $\Omega_b h^2 = 0.025 \pm 0.001$, and the Kirkman et al. (2003) estimate of $\Omega_b h^2 = 0.0214 \pm 0.0020$ The remarkable agreement between the baryon density inferred from D/H values and our measurements is an important triumph for the basic big bang model.

4.4. *Cosmic Ages*

The age of the universe based on the best fit to *WMAP* data only, $t_0 = 13.4 \pm 0.3$ Gyr. However, the addition of other data sets (see § 5) implies a lower matter density and a slightly larger age. The best-fit age for the power-law model based on a combination of *WMAP*, 2dFGRS, and Lyα forest data is $t_0 = 13.6 \pm 0.2$ Gyr. The best-fit age for the same data set for the running index model of § 5.2 is $t_0 = 13.7 \pm 0.2$ Gyr. (See Hu et al. 2001 and Knox, Christensen, & Skordis 2001 for discussions of using CMB data to determine cosmological ages.)

A lower limit to the age of the universe can independently be obtained from dating the oldest stellar populations. This has been done traditionally by dating the oldest stars in the Milky Way (see e.g., Chaboyer 1998; Jimenez 1999).

For this program, globular clusters are an excellent laboratory for constraining the age of the universe: each cluster has a chemically homogeneous population of stars all born nearly simultaneously. The main uncertainty in the age determination comes from the poorly known distance (Chaboyer 1995). Well-understood stellar populations are useful tools for constraining cluster distances: Renzini et al. (1996) used the white dwarf sequence to obtain an age of 14.5 ± 1.5 Gyr for NGC 6752. Jimenez et al. (1996), using a distance-independent method, determined the age of the oldest globular clusters to be 13.5 ± 2 Gyr. Using the luminosity function method, Jimenez & Padoan (1998) found an age of 12.5 ± 1.0 Gyr for M55. This method gives a joint constraint on the distance and the age of the globular cluster. Other groups find consistent ages: Gratton et al. (1997) estimate an age of $11.8^{+2.1}_{-2.5}$ Gyr for the oldest Galactic globular clusters; VandenBerg et al. (2002) estimate an age of ∼13.5 Gyr for M92. Krauss & Chaboyer (2003) review the globular cluster analysis and quote a best-fit age of 13.4 Gyr.

Observations of eclipsing double line spectroscopic binaries enable globular cluster age determinations that avoid the considerable uncertainty associated with the globular cluster distance scale (Paczyński 1997). Thompson et al. (2001) were able to obtain a high-precision mass estimate for the detached double line spectroscopic binary, OGLE GC-17 in ω Cen. Using the age/turnoff mass relationship, the Kaluzny et al. (2002) analysis of this system yielded an age for this binary of 11.8 ± 0.6 Gyr. The Chaboyer & Krauss (2002) reanalysis of the age/turnoff mass relationship for this system yields a similar age estimate: 11.1 ± 0.67 Gyr. The *WMAP* determination of the age of the universe implies that globular clusters form within 2 Gyr after the big bang, a reasonable estimate that is consistent with structure formation in the ΛCDM cosmology.

White dwarf dating provides an alternative approach to the traditional studies of the main-sequence turnoff. Richer et al. (2002) and Hansen et al. (2002) find an age for the globular cluster M4 of 12.7 ± 0.7 Gyr ($2\,\sigma$ errors, ± 0.35 at the $1\,\sigma$ level assuming Gaussian errors) using the white dwarfs cooling sequence method. These results, which yield an age close to the cosmological age, are potentially very useful: further tests of the assumptions of the white dwarf age dating method will clarify its systematic uncertainties.

Observations of nearby halo stars enable astronomers to obtain spectra of various radioisotopes. By measuring isotopic ratios, they infer stellar ages that are independent of much of the physics that determines main-sequence turnoff (see Thielemann et al. 2002 for a recent review). These studies yield stellar ages consistent with both the globular cluster ages and the ages in our best-fit models. Clayton (1988), using a range of chemical evolution models for the Galaxy, finds ages between 12 and 20 Gyr. Schatz et al. (2002) study thorium and uranium in CS 31082-001 and estimate an age of 15.5 ± 3.2 Gyr for the *r*-process elements in the star. Other groups find similar estimates: the Cayrel et al. (2001) analysis of U-238 in the old halo star CS 31082-001 yields an age of 12.5 ± 3 Gyr, while Hill et al. (2002) find an age of 14.0 ± 2.4 Gyr. Studies of other old halo stars yield similar estimates: Cowan et al. (1999), using the two stars CS 22892-052 and HD 115444, find 15.6 ± 4.6 Gyr.

Table 6 summarizes the lower limits on the age of the universe from various astronomical measurements. While the errors on these measurements remain too large to effectively constrain parameters, they provide an important consistency check on our basic cosmological model.

TABLE 6
COSMIC AGE

Method	Age (Gyr)
WMAP data (ΛCDM)	13.4 ± 0.3
*WMAP*ext+2dFGRS	13.7 ± 0.2
Globular cluster ages	>11–16
White dwarf	$>12.7 \pm 0.7$
OGLE GC-17	>10.4–12.8
Radioactive dating	>9.5–20

4.5. *Large-Scale Structure*

The large-scale structure observations and the Lyα forest data complement the CMB measurements by measuring similar physical scales at very different epochs. The *WMAP* angular power spectrum has the smallest uncertainties near $\ell \sim 300$, which correspond to wavenumbers $k \sim 0.02$ Mpc^{-1}. With the ACBAR results, our CMB data set extends to $\ell \sim 1800$, corresponding to $k \sim 0.1$ Mpc^{-1}. If we assume that gravity is the primary force determining the large-scale distribution of matter and that galaxies trace mass at least on large scales, then we can directly compare our best-fit ΛCDM model (with parameters fit to the *WMAP* data) to observations of large-scale distribution of galaxies. There are currently two major ongoing large-scale structure surveys: the 2dFGRS; Colless et al. 2001), and the SDSS.[14] Large-scale structure data sets are a powerful tool for breaking many of the parameter degeneracies associated with CMB data. In § 5, we make extensive use of the 2dFGRS data set.

Figure 6 shows that the ΛCDM model obtained from the *WMAP* data alone is an acceptable fit to the 2dFGRS power spectrum. The best fit has $\beta = 0.45$, consistent with the Peacock et al. (2001) measured value of $\beta = 0.43 \pm 0.07$.

The Lyα forest observations are an important complement to CMB observations since they probe the linear matter power spectrum at $z = 2$–3 (Croft et al. 1998, 2002). These observations are sensitive to small length scales, inaccessible to CMB experiments. Unfortunately, the relationship between the measured flux power spectrum and the linear power spectrum is complex (Gnedin & Hamilton 2002; Croft et al. 2002) and needs to be calibrated by numerical simulations. In Verde et al. (2003), we describe our methodology for incorporating the Lyα forest data into our likelihood approach. Figure 6 compares the predicted power spectra for the best-fit ΛCDM model to the linear power spectra inferred by Gnedin & Hamilton (2002) and by Croft et al. (2002).

[14] http://www.sdss.org.

4.6. *Supernova Data*

Over the past decade, Type Ia supernovae have emerged as important cosmological probes. Once supernova light curves have been corrected using the correlation between decline rate and luminosity (Phillips 1993; Riess et al. 1995), they appear to be remarkably good standard candles. Systematic studies by the supernova cosmology project (Perlmutter et al. 1999) and by the high z supernova search team (Riess et al. 1998) provide evidence for an accelerating universe. The combination of the large-scale structure, CMB, and supernova data provide strong evidence for a flat universe dominated by a cosmological constant (Bahcall et al. 1999). Since the supernova data probes the luminosity distance versus redshift relationship at moderate redshift $z < 2$ and the CMB data probes the angular diameter distance relationship to high redshift ($z \sim 1089$), the two data sets are complementary. The supernova constraint on cosmological parameters are consistent with the ΛCDM *WMAP* model. As we will see in the discussion of nonflat models and quintessence models, the Type Ia supernova likelihood surface in the Ω_m-Ω_Λ and in the Ω_m-ω planes provides useful additional constraints on cosmological parameters.

4.7. *Reionization and Small-Scale Power*

The *WMAP* detection of reionization (Kogut et al. 2003) implies the existence of an early generation of stars able to reionize the universe at $z \sim 20$. Is this early star formation compatible with our best-fit ΛCDM cosmological model? We can evaluate this effect by first computing the fraction of collapsed objects, $f_{\rm DM}$, at a given redshift:

$$f_{\rm DM}(z) = \frac{1}{\rho_0} \int_{M_{\rm min}}^{\infty} \Phi(M, z) M \, dM \ , \qquad (2)$$

where $\Phi(M, z)$ is the Sheth & Tormen (1999) mass function. The first stars correspond to extremely rare fluctuations of the overdensity field: equation (2) is very sensitive to the tail of the mass function. Thus the very small change in the minimum mass needed for star formation results in a significant change in the fraction of collapsed objects. The minimum

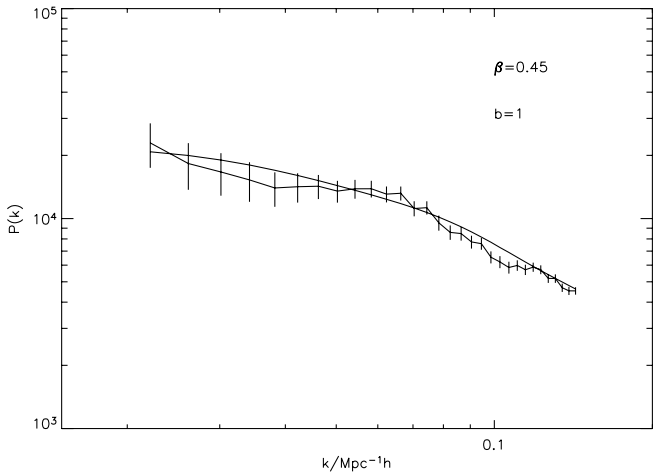

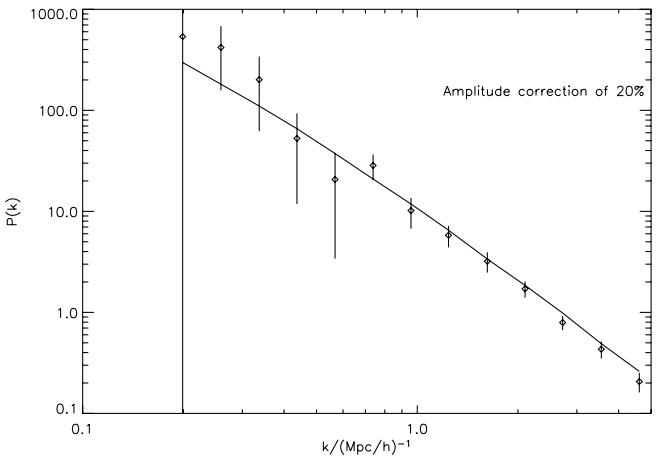

FIG. 6.—*Left*: Comparison of the best-fit ΛCDM model of § 3 based on *WMAP* data only to the 2dFGRS power spectrum (Percival et al. 2001). The bias parameter for the best-fit power-law ΛCDM model is 1.0, corresponding to a best-fit value of $\beta = 0.45$. *Right*: Comparison of the best-fit power-law ΛCDM model of § 3 to the power spectrum at $z = 3$ inferred from the Lyα forest data. The data points have been scaled downward by 20%, which is consistent with the 1 σ calibration uncertainty (Croft et al. 2002).

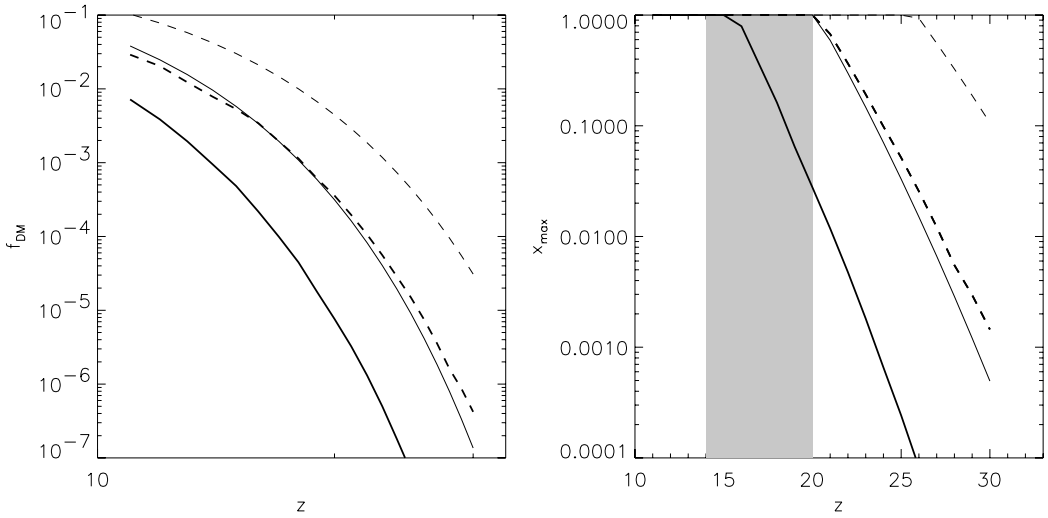

FIG. 7.—*Left*: Fraction of mass in bound objects as a function of redshift. The black lines show the mass in collapsed objects with mass greater than $M^{\rm HRL}(z)$, the effective Jeans mass in the absence of H_2 cooling for our best-fit PL ΛCDM model (thin lines are for the fit to *WMAP* only, and thick lines are for the fit to all data sets). The heavy line uses the best-fit parameters based on all data (which has a lower σ_8), and the light line uses the best-fit parameters based on fitting to the *WMAP* data only. The dashed lines show the mass in collapsed objects with masses greater than the Jeans mass assuming that the minimum mass is $10^6\ M_\odot$. More objects form if the minimum mass is lower. *Right*: Ionization fraction as a function of redshift. The solid line shows ionization fraction for the best-fit PL ΛCDM model if we assume that H_2 cooling is suppressed by photodestruction of H_2. This figure suggests that H_2 cooling may be necessary for enough objects to form early enough to be consistent with the *WMAP* detection. The heavy line is for the best-fit parameters for all data sets, and the light line is for the best-fit parameters for the *WMAP* only fit. The dashed lines assume that the objects with masses greater than $10^6\ M_\odot$ can form stars. The gray band shows the 68% likelihood region for z_r based on the assumption of instantaneous complete reionization (Kogut et al. 2003).

halo mass for star formation, $M_{\rm min}$, is controversial and depends on whether molecular hydrogen (H_2) is available as a coolant. If the gas temperature is fixed to the CMB temperature, then the Jeans mass, $M^{\rm J} = 10^6\ M_\odot$. If molecular hydrogen is available, then the Jeans mass before reionization is $M^{\rm J'} \sim 2.2 \times 10^3 [w_b/h(w_m)]^{1.5}(1+z)/10$ for $z < 150$ (Venkatesan et al. 2001). At $z > 150$, the electrons are thermally coupled to the CMB photons. However, as Haiman et al. (1997) point out, a small UV background generated by the first sources will dissociate H_2, thus making the minimum mass much larger than the Jeans mass. They suggest using a minimum mass that is much higher: $M_{\rm min}^{\rm HRL}(z) = [10^8(1+z)/10]^{-3/2}$. On the other hand, if the first stars generated a significant flux of X-rays (Oh 2001), then this would have promoted molecular hydrogen formation (Haiman et al. 2000; Venkatesan et al. 2001; Cen 2002), thus lowering the minimum mass back to $M^{\rm J}$.

Following Tegmark & Silk (1995) we estimate the rate of reionization by multiplying the collapse factor by an efficiency factor. A fraction of baryons in the universe, f_b, falls into the nonlinear structures. We assume $f_b = f_{\rm DM}$ (i.e., constant baryon/dark matter ratio). A certain fraction of these baryons form stars or quasars, $f_{\rm burn}$, which emit UV radiation with some efficiency, $f_{\rm UV}$. Some of this radiation escapes into the intergalactic medium photoionizing it; however, the net number of ionizations per UV photons, $f_{\rm ion}$, is expected to be less than unity (due to cooling and recombinations). Finally, the intergalactic medium might be clumpy, making the photoionization process less efficient. This effect is counted for by the clumping factor $C_{\rm clump}$. Thus in this approximation the ionization fraction is given by $x_e = 3.8 \times 10^5 f_{\rm net} f_b$, where $f_{\rm net} = f_{\rm burn} f_{\rm UV} f_{\rm esc} f_{\rm ion}/C_{\rm clump}$. The factor 3.8×10^5 arises because 7.3×10^{-3} of the rest mass is released in the burning of hydrogen to helium and we assume the primordial helium mass fraction to be 24%. We assume $f_{\rm burn} \lesssim 25\%$, $f_{\rm esc} \lesssim 50\%$, $f_{\rm UV} \lesssim 50\%$, $f_{\rm ion} \lesssim 90\%$, and $1 \lesssim C_{\rm clump} \lesssim 100$, thus $f_{\rm net} \lesssim 5.6 \times 10^{-3}$.

Figure 7 shows the fraction of collapsed objects and the maximum ionization fraction as a function of redshift for our best-fit *WMAP* ΛCDM model. The solid lines correspond to $M_{\rm min} = M_{\rm min}^{\rm HRL}(z)$, while the dashed lines correspond to $M_{\rm min} = M^{\rm J}$. The *WMAP* detection of reionization at high redshift suggests that H_2 cooling likely played an important role in early star formation.

Because early reionization requires the existence of small-scale fluctuations, the *WMAP* TE detection has important implications for our understanding of the nature of the dark matter.

Barkana et al. (2001) note that the detection of reionization at $z > 10$ rules out warm dark matter as a viable candidate for the missing mass as structure forms very late in these models. Warm dark matter cannot cluster on scales smaller than the dark matter Jeans mass. Thus, this limit applies regardless of whether the minimum mass is $M^{\rm HRL}$ or $M^{\rm J}$.

5. COMBINING DATA SETS

In this section, we combine the *WMAP* data with other CMB experiments that probe smaller angular scales (ACBAR and CBI)[15] and with astronomical measurements of the power spectrum (the 2dFGRS and Lyα forest). We begin by exploring how including these data sets affects our best-fit power-law ΛCDM model parameters (§ 5.1). The addition of data sets that probe smaller scales systematically pulls down the amplitude of the fluctuations in the best-fit

[15] In the following sections, we refer to the combined *WMAP*, ACBAR. and CBI data sets as *WMAP*ext.

TABLE 7
BEST-FIT PARAMETERS: POWER-LAW ΛCDM MODEL

Parameter	*WMAP*	*WMAP*ext[a]	*WMAP*ext+2dFGRS	*WMAP*ext+2dFGRS+Lyα
A	0.9 ± 0.1	0.8 ± 0.1	0.8 ± 0.1	$0.75^{+0.08}_{-0.07}$
n_s	0.99 ± 0.04	0.97 ± 0.03	0.97 ± 0.03	0.96 ± 0.02
τ	$0.166^{+0.076}_{-0.071}$	$0.143^{+0.071}_{-0.062}$	$0.148^{+0.073}_{-0.071}$	$0.117^{+0.057}_{-0.053}$
h	0.72 ± 0.05	0.73 ± 0.05	0.73 ± 0.03	0.72 ± 0.03
$\Omega_m h^2$	0.14 ± 0.02	0.13 ± 0.01	0.134 ± 0.006	0.133 ± 0.006
$\Omega_b h^2$	0.024 ± 0.001	0.023 ± 0.001	0.023 ± 0.001	0.0226 ± 0.0008
$\chi^2_{\rm eff}/\nu$	1431/1432	1440/1352	1468/1381	...[b]

[a] *WMAP*+CBI+ACBAR.
[b] Since the Lyα data points are correlated, we do not quote an effective χ^2 for the combined likelihood including Lyα data (see Verde et al. 2003).

model. This motivates our exploration of an extension of the power-law model, a model in which the primordial power spectrum of scalar density fluctuations is fitted by a running spectral index (Kosowsky & Turner 1995):

$$P(k) = P(k_0)\left(\frac{k}{k_0}\right)^{n_s(k_0)+(1/2)dn_s/d\ln k \ln(k/k_0)}, \qquad (3)$$

where we fix the scalar spectral index and slope at $k_0 = 0.05$ Mpc^{-1}. Note that this definition of the running index matches the definition used in Hannestad et al. (2002) analysis of running spectral index models and differs by a factor of 2 from the Kosowsky & Turner (1995) definition. As in the scale independent case, we define

$$n_s(k) = \frac{d\ln P}{d\ln k}. \qquad (4)$$

We explicitly assume that $d^2 n_s/d\ln k^2 = 0$, so that

$$n_s(k) = n_s(k_0) + \frac{dn_s}{d\ln k}\ln\left(\frac{k}{k_0}\right). \qquad (5)$$

In § 5.2, we show that the running spectral index model is a better fit than the pure power-law model to the combination of *WMAP* and other data sets. Peiris et al. (2003) explore the implications of this running spectral index for inflation.

5.1. *Power-Law CDM Model*

The power-law ΛCDM model is an acceptable fit to the *WMAP* data. While it overpredicts the amplitude of fluctuations on large angular scales (see § 6), this deviation may be due to cosmic variance at these large scales. Intriguingly, it also overpredicts the amplitude of fluctuations on small angular scales.

Table 7 shows the best-fit parameters for the power-law ΛCDM model for different combination of data sets. As we add more and more data on smaller scales, the best-fit value for the amplitude of fluctuations at $k = 0.05$ Mpc^{-1} gradually drops: When we fit to the *WMAP* data alone, the best fit is 0.9 ± 0.1. When we add the CBI, ACBAR, and 2dFGRS data, the best-fit value drops to 0.8 ± 0.1. Adding the Lyα data further reduces A to $0.75^{+0.08}_{-0.07}$. The best-fit spectral index shows a similar trend: the addition of more and more small-scale data drives the best-fit spectral index to also change by nearly $1\,\sigma$ from its best-fit value for *WMAP* data only: 0.99 ± 0.04 (*WMAP* only) to 0.96 ± 0.02 (*WMAP*ext+2dFGRS+Lyα). When the addition of new data continuously pulls a model away from its best-fit value, this is often the signature of the model requiring a new parameter.

5.2. *Running Spectral Index ΛCDM Model*

Inflationary models predict that the spectral index of fluctuations should be a slowly varying function of scale. Peiris et al. (2003) discuss the inflationary predictions and shows that a plausible set of models predicts a detectable varying spectral index. There are classes of inflationary models that predict minimal tensor modes. This section explores this class of models. In § 6.4, we explore a more general model that has both a running spectral index and tensor modes.

Table 8 shows the best-fit parameters for the running (RUN) spectral index model as a function of data set. Note that the best-fit parameters for these models barely change

TABLE 8
BEST-FIT PARAMETERS FOR THE RUNNING SPECTRAL INDEX ΛCDM MODEL

Parameter	*WMAP*	*WMAP*ext	*WMAP*ext +2dFGRS	*WMAP*ext+2dFGRS+Lyα
A	0.92 ± 0.12	0.9 ± 0.1	0.84 ± 0.09	$0.83^{+0.09}_{-0.08}$
n_s	$0.93^{+0.07}_{-0.07}$	0.91 ± 0.06	$0.93^{+0.04}_{-0.05}$	0.93 ± 0.03
$dn_s/d\ln k$	-0.047 ± 0.04	-0.055 ± 0.038	$-0.031^{+0.023}_{-0.025}$	$-0.031^{+0.016}_{-0.017}$
τ	0.20 ± 0.07	0.20 ± 0.07	0.17 ± 0.06	0.17 ± 0.06
h	0.70 ± 0.05	0.71 ± 0.06	0.71 ± 0.04	$0.71^{+0.04}_{-0.03}$
$\Omega_m h^2$	0.14 ± 0.02	0.14 ± 0.01	0.136 ± 0.009	$0.135^{+0.008}_{-0.009}$
$\Omega_b h^2$	0.023 ± 0.002	0.022 ± 0.001	0.022 ± 0.001	0.0224 ± 0.0009
$\chi^2_{\rm eff}/\nu$	1429/1431	1437/1351	1465/1380	*[a]

[a] Since the Lyα data points are correlated, we do not quote $\chi^2_{\rm eff}$ for the combined likelihood including Lyα data (see Verde et al. 2003).

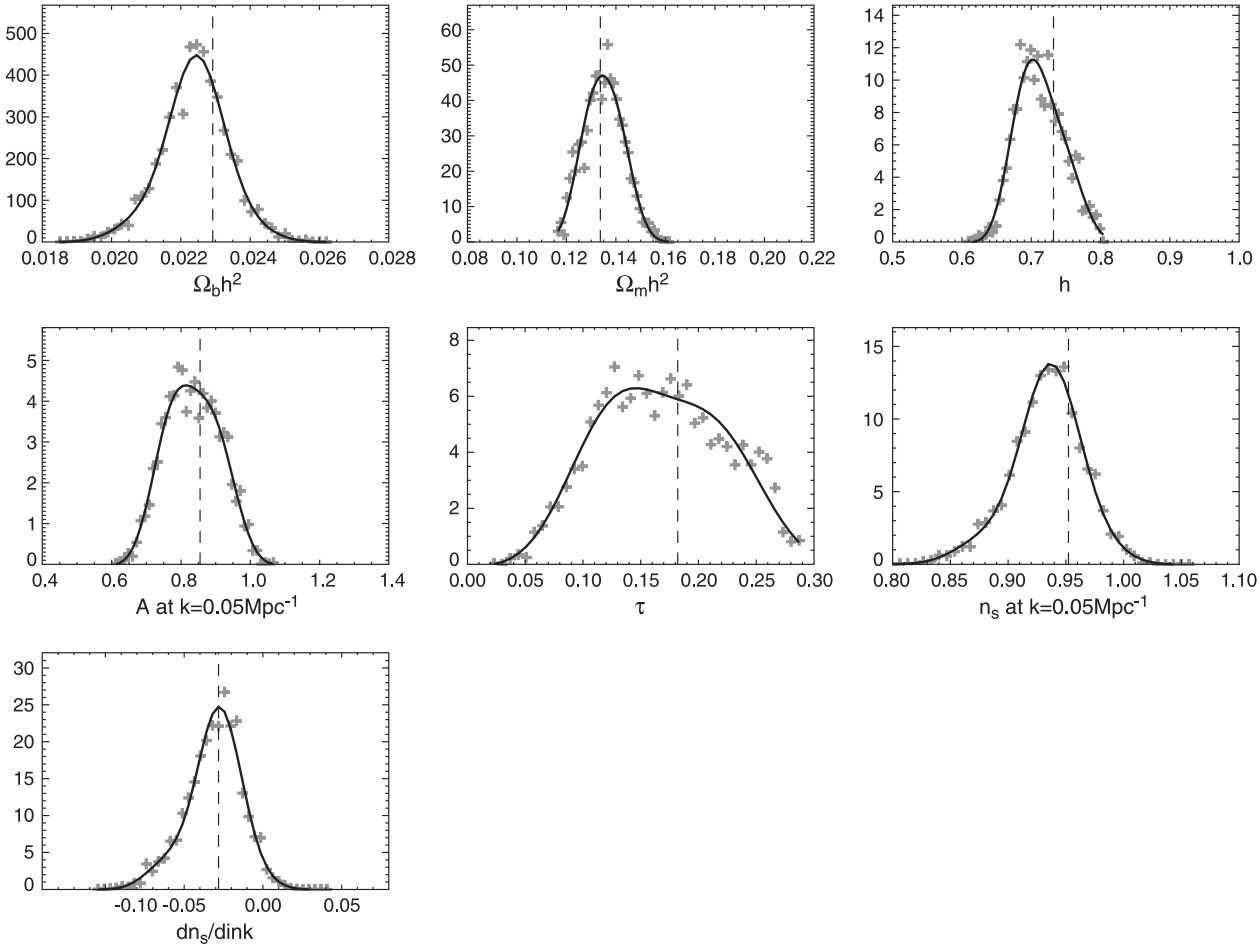

FIG. 8.—Marginalized likelihood for various cosmological parameters in the running spectral index model for our analysis of the combined *WMAP*, CBI, ACBAR, 2dFGRS, and Lyα data sets. The dashed lines show the maximum-likelihood values of the global seven-dimensional fit.

as we add new data sets; however, the error bars shrink (see Fig. 8). When we include all data sets, the best-fit value of the running of the spectral index is $-0.031^{+0.016}_{-0.017}$: fewer than 5% of the models have $dn_s/d\ln k > 0$.

Figure 9 shows the power spectrum as a function of scale. The figure shows the results of our Markov chain analysis of the combination of *WMAP*, CBI, ACBAR, 2dFGRS, and Lyα data. At each wavenumber, we compute the range of values for the power-law index for all of the points in the Markov chain. The 68% and 95% contours at each k value are shown in Figure 9 for the fit to the *WMAP*ext+2dFGRS+Lyα data sets.

Over the coming year, new data will significantly improve our ability to measure (or constrain) this running spectral index. When we complete our analysis of the EE power spectrum, the *WMAP* data will place stronger constraints on τ. Because of the n_s-τ degeneracy, this implies a strong constraint on n_s on large scales. The SDSS collaboration will soon release its galaxy spectrum and its measurements of the Lyα forest. These observations will significantly improve our measurements of n_s on small scales. Peiris et al. (2003) show that the detection of a running spectral index and particularly the detection of a spectral index that varies from $n_s > 1$ on large scales to $n_s < 1$ on small scales would severely constrain inflationary models.

The running spectral index model predicts a significantly lower amplitude of fluctuations on small scales than the standard ΛCDM model (see Fig. 9). This suppression of small-scale power has several important astronomical implications: (1) the reduction in small-scale power makes it more difficult to reionize the universe unless H_2 cooling enables mass dark halos to collapse and form galaxies (see § 4.7 and Fig. 10); (2) a reduction in the small-scale power reduces the amount of substructure within galactic halos (Zentner & Bullock 2002); and (3) since small objects form later, their dark matter halos will be less concentrated as there is a monotonic relationship between collapse time and halo central concentration (Navarro et al. 1997; Eke et al. 2001; Zentner & Bullock 2002; Wechsler et al. 2002; Huffenberger & Seljak 2003). The reduction in the amount of substructure will also reduce angular momentum transport between dark matter and baryons and will also reduce the rate of disk destruction through infall (Toth & Ostriker 1992). We suspect that our proposed modification of the primordial power spectrum will resolve many of the long-standing problems of the CDM model on small scales (see Moore 1994 and Spergel & Steinhardt 2000 for discussions of the failings of the power-law ΛCDM model on galaxy scales).

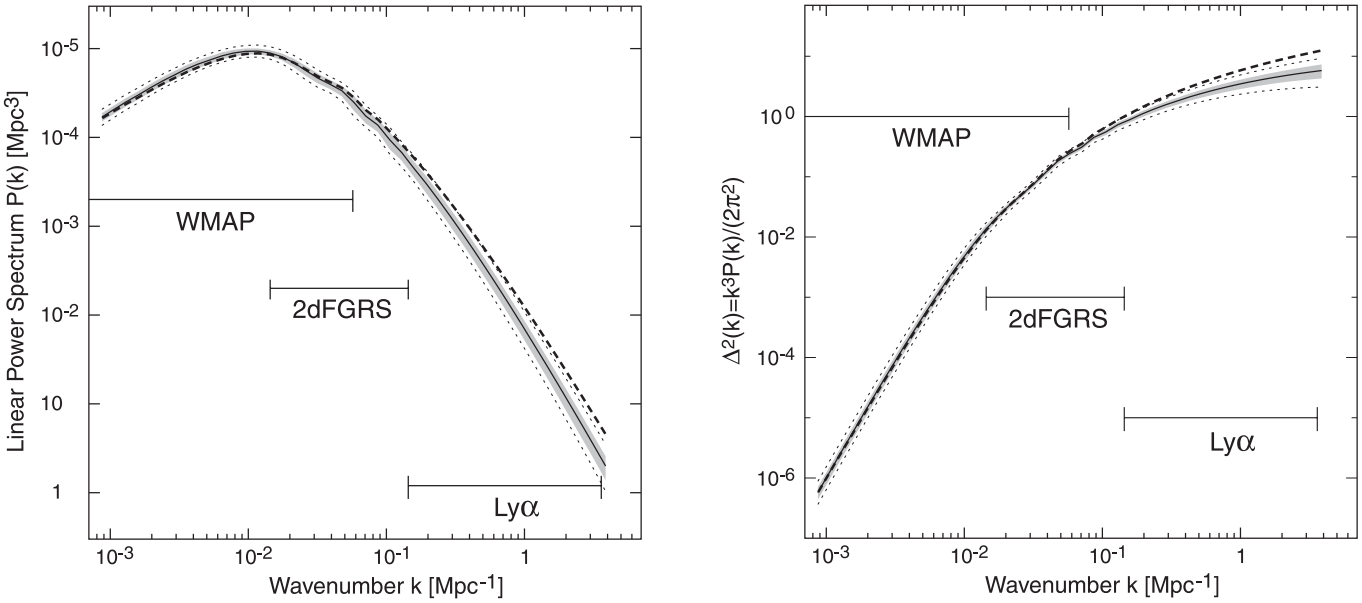

FIG. 9.—*Left*: The shaded region in the figure shows the 1 σ contours for the amplitude of the power spectrum as a function of scale for the running spectral index model fit to all data sets. The dotted lines bracket the 2 σ region for this model. The dashed line is the best-fit power spectrum for the power-law ΛCDM model. *Right*: The shaded region in the figure shows the 1 σ contours for the amplitude of the amplitude of mass fluctuations, $\Delta^2(k) = k^3P(k)/(2\pi^2)$, as a function of scale for the running spectral index model fit to all data sets. The dotted lines bracket the 2 σ region for this model. The dashed line is the best fit for the power-law ΛCDM model.

6. BEYOND THE ΛCDM MODEL

In this section, we consider various extensions to the ΛCDM model. In § 6.1, we consider dark energy models with a constant equation of state. In § 6.2, we consider nonflat models. In § 6.3, we consider models with a massive light neutrino. In § 6.4, we include tensor modes.

In this section of the paper, we combine the *WMAP* data with external data sets so that we can break degeneracies and obtain significant constraints on the various extensions of our standard cosmological model.

6.1. *Dark Energy*

The properties of the dark energy, the dominant component in our universe today, is a mystery. The most popular alternative to the cosmological constant is quintessence. Wetterich (1988), Ratra & Peebles (1988), and Peebles &

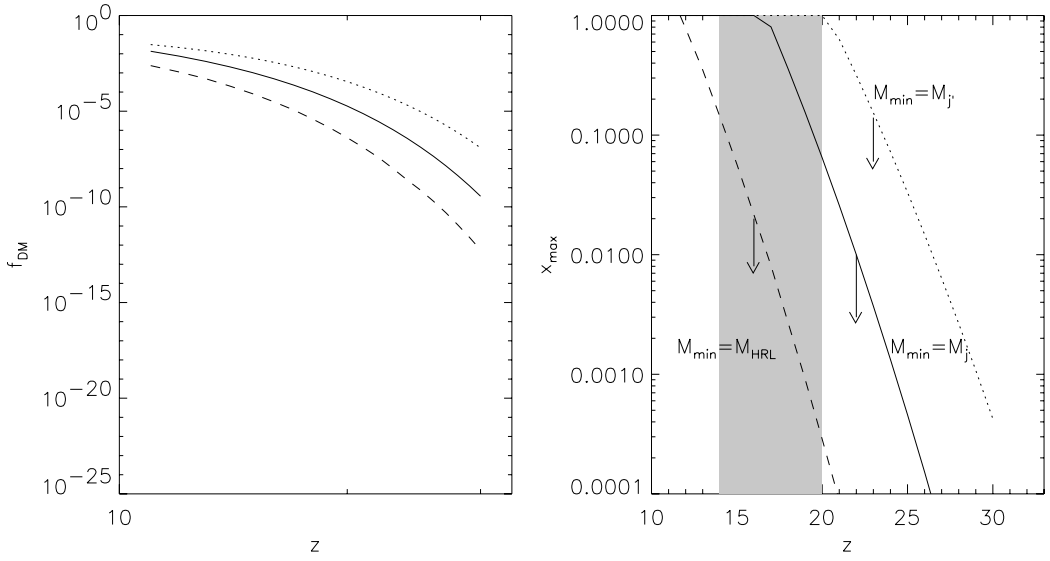

FIG. 10.—*Left*: Fraction of the universe in bound objects with mass greater than $M^{\rm HRL}$ (*dashed line*), $M^j = 10^6\ M_\odot$ (*solid line*), and $M^{j'}$ (*dotted line*) in a model with a running spectral index. The curves were computed for the 1 σ upper limit parameters for this model (see Fig. 9). These should be viewed as upper limits on the mass fraction in collapsed objects. *Right*: Ionization fraction as a function of redshift and is based on the assumptions described in § 4.7. As in the left panel, we use the 1 σ upper limit estimate of the power spectrum so that we obtain "optimistic" estimates of the reionization fraction. In the context of a running spectral index fit to the data, the *WMAP* detection of reionization appears to require that H_2 cooling played an important role in early star formation.

Ratra (1988) suggest that a rolling scalar field could produce a time-variable dark energy term, which leaves a characteristic imprint on the CMB and on large-scale structure (Caldwell et al. 1998). In these quintessence models, the dark energy properties are quantified by the equation of state of the dark energy: $w = p/\rho$, where p and ρ are the pressure and the density of the dark energy. A cosmological constant has an equation of state, $w = -1$.

Since the space of possible models is quite large, we only consider models with a constant equation of state. We now increase our model space so that we have seven parameters in the cosmological model (A, n_s, h, Ω_m, Ω_b, τ, and w). We analyze the data using two approaches: (1) we begin by restricting our analysis to $w > -1$ motivated by the difficulties in constructing stable models with $w < -1$ (Carroll et al. 2003), and (2) we relax this constraint and consider models that violate the weak energy condition (Schuecker et al. 2003b). We have included perturbations (clustering) in the dark energy, assuming that the speed of sound of the dark energy equals the speed of light. This assumption is valid for the dark energy component made of a scalar field with canonical form of the kinetic energy density. Further analysis is needed for models where w and the quintessence sound speed are a function of time (Dedeo et al. 2003). The addition of a new parameter introduces a new degeneracy between Ω_m, h, and w that cannot be broken by CMB data alone (Huey et al. 1999; Verde et al. 2003): models with the same values of $\Omega_m h^2$, $\Omega_b h^2$, and first peak position have nearly identical angular power spectra.

For example, a model with $\Omega_m = 0.47$, $w = -\frac{1}{2}$ and $h = 0.57$ has a nearly identical angular power spectrum to our ΛCDM model. Note, however, that this Hubble constant value differs by 2 σ from the *HST* Key Project value and the predicted shape of the power spectrum is a poor fit to the 2dFGRS observations. This model is also a worse fit to the supernova angular diameter distance relation.

We consider four different combinations of astronomical data sets: (1) *WMAP*ext data combined with the supernova observations, (2) *WMAP*ext data combined with *HST* data, (3) *WMAP*ext data combined with the 2dFGRS large-scale structure data, and (4) all data sets combined.

The CMB peak positions constrain the conformal distance to the decoupling surface. The amplitude of the early ISW signal determines the matter density, $\Omega_m h^2$. The combination of these two measurements strongly constrains $\Omega(w)$ and $h(w)$ (see Figs. 11 and 12). The *HST* Key Project measurement of H_0 agrees with the inferred CMB value if $w = -1$. As w increases, the best-fit H_0 value for the CMB drops below the Key Project value. Our joint analysis of CMB+*HST* Key Project data implies that $w < -0.5$ (95%

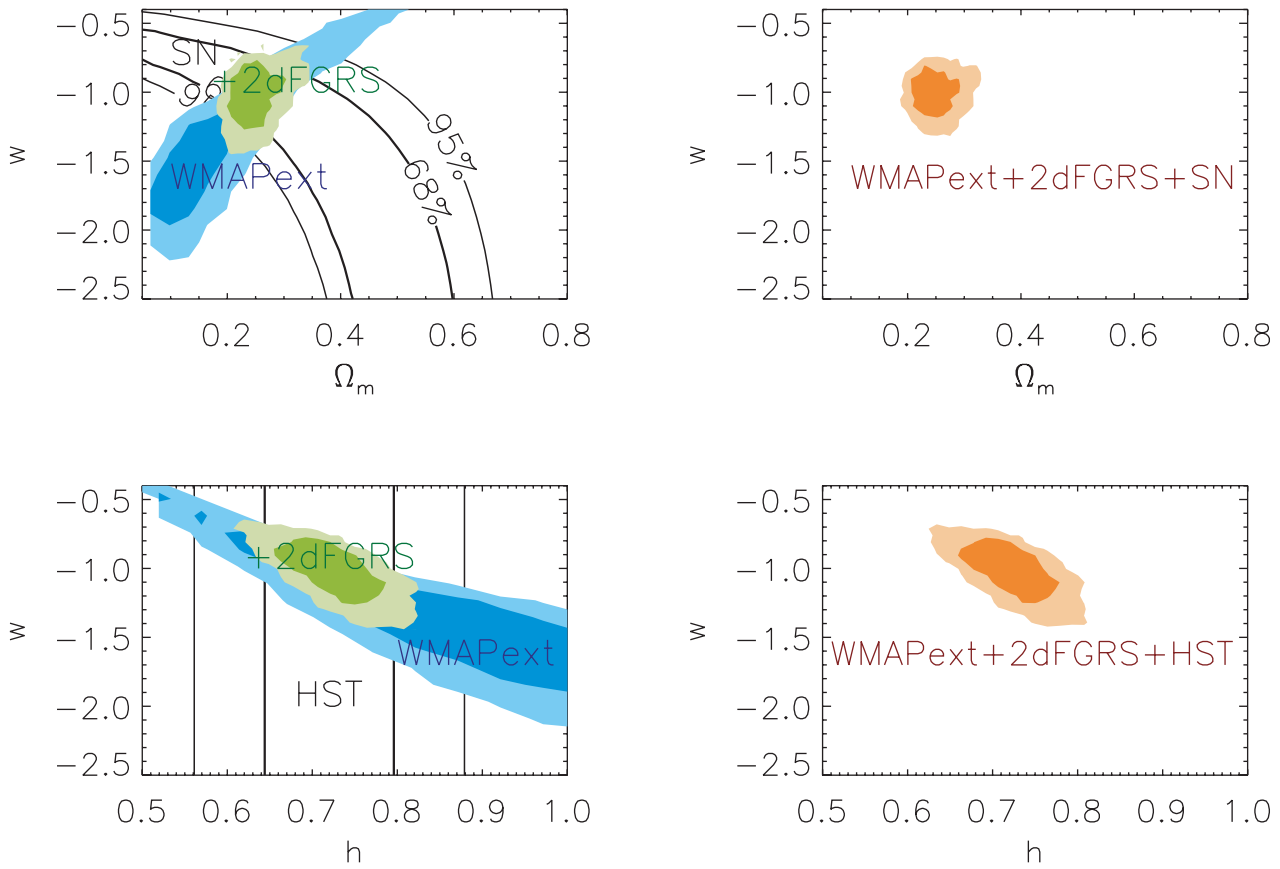

FIG. 11.—Constraints on dark energy properties. The upper left panel shows the marginalized maximum-likelihood surface for the *WMAP*ext data alone and for a combination of the *WMAP*ext+2dFGRS data sets. The solid lines in the figure show the 68% and 95% confidence ranges for the fit C supernova data from Perlmutter et al. (1999). In the upper right panel, we multiply the supernova likelihood function by the *WMAP*ext+2dFGRS likelihood functions. The lower left panel shows the maximum-likelihood surface for h and w for the *WMAP*ext data alone and for the *WMAP*ext+2dFGRS data sets. The solid lines in the figures are the 68% and 95% confidence limits on H_0 from the *HST* Key Project, where we add the systematic and statistical errors in quadrature. In the lower right panel, we multiply the likelihood function for the *WMAP*ext+2dFGRS data by the likelihood surface for the *HST* data to determine the joint likelihood surface. The dark areas in these plots are the 68% likelihood regions, and the light areas are the 95% likelihood regions.

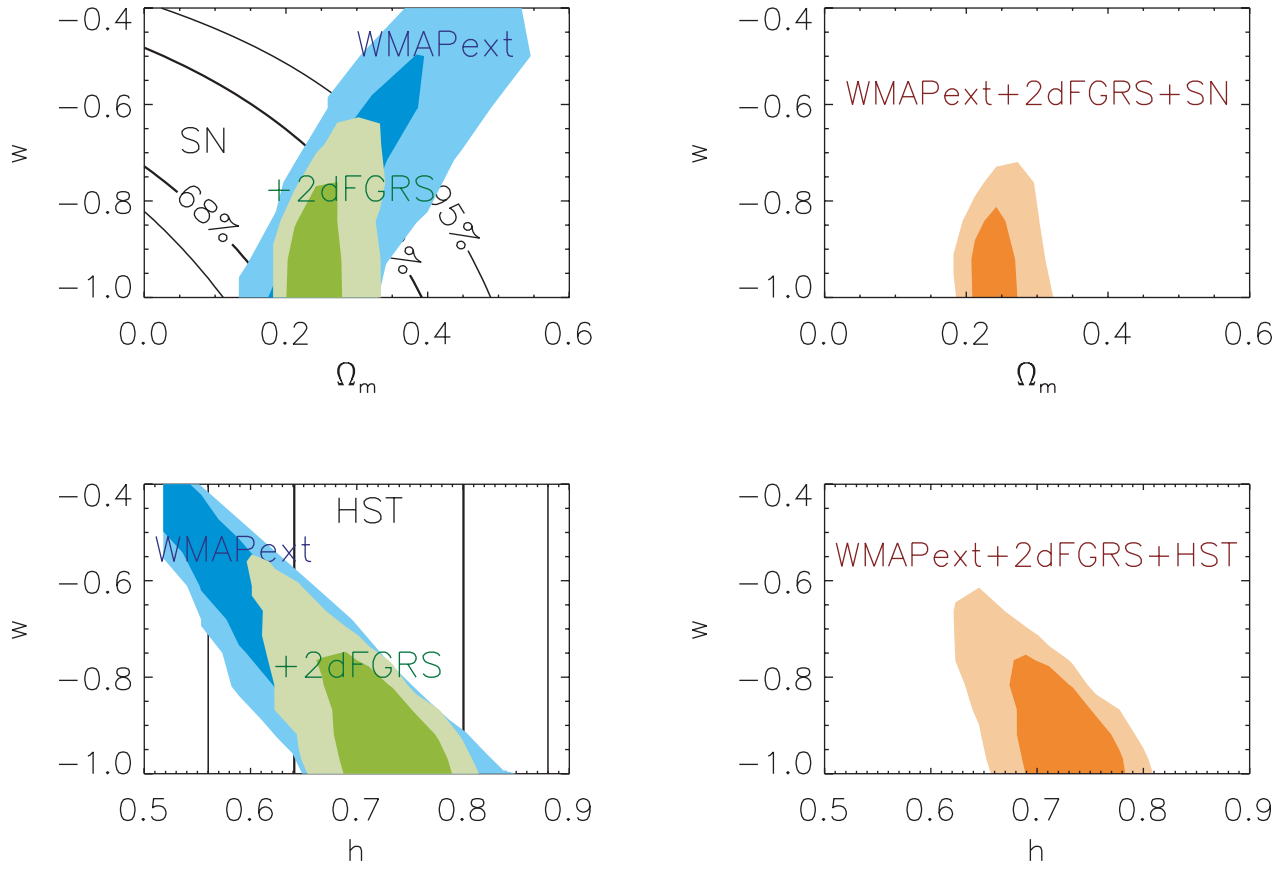

FIG. 12.—Constraints on dark energy properties. The upper left panel shows the marginalized maximum-likelihood surface for the *WMAP*ext data alone and for a combination of the *WMAP*ext+2dFGRS data sets. The solid lines in the figure show the 68% and 95% confidence ranges for supernova data from Riess et al. (2001). In the upper right panel, we multiply the supernova likelihood function by the *WMAP*ext+2dFGRS likelihood functions. The lower left panel shows the maximum-likelihood surface for h and w for the *WMAP*ext data alone and for the *WMAP*ext+2dFGRS data sets. The solid lines in the figures are the 68% and 95% confidence limits on H_0 from the *HST* Key Project, where we add the systematic and statistical errors in quadrature. In the lower right panel, we multiply the likelihood function for the *WMAP*ext+2dFGRS data by the likelihood surface for the *HST* data to determine the joint likelihood surface. The dark areas in these plots are the 68% likelihood regions, and the light areas are the 95% likelihood regions. The calculations for this figure assumed a prior that $w > -1$.

confidence interval). If future observations can reduce the uncertainties associated with the distance to the LMC, the H_0 measurements could place significantly stronger limits on w. Figures 11 and 12 show that the combination of either CMB+supernova data or CMB+large-scale structure data place similar limits on dark energy properties. For our combined data set, we marginalize over all other parameters and find that $w < -0.78$ (95% c.l.) when we impose the prior that $w > -1$. If we drop this prior, then all of the combined data sets appear to favor a model where the properties of the dark energy are close to the predicted properties of a cosmological constant ($w = -0.98 \pm 0.12$).

6.2. *Nonflat Models*

The position of the first peak constrains the universe to be nearly flat (Kamionkowski et al. 1994); low-density models with $\Omega_\Lambda = 0$ have their first peak position at $\ell \sim 200\Omega_m^{-1/2}$. However, if we allow for the possibility that the universe is nonflat and there is a cosmological constant, then there is a geometric degeneracy (Efstathiou & Bond 1999): along a line in Ω_m-Ω_Λ space, there is a set of models with nearly identical angular power spectra. While the allowed range of $\Omega_{\rm tot}$ is relatively small, there is a wide range in Ω_m values compatible with the CMB data in a nonflat universe.

If we place no priors on cosmological parameters, then there is a model with $\Omega_\Lambda = 0$ consistent with the *WMAP* data ($\Delta\chi^2 = 6.6$ relative to the flat model). However, the cosmological parameters for this model ($H_0 = 32.5$ km s^{-1} Mpc^{-1} and $\Omega_{\rm tot} = 1.28$) are violently inconsistent with a host of astronomical measurements. The flat $\Omega_m = 1, \Lambda = 0$ standard CDM model is inconsistent with the *WMAP* data at more than the 5 σ level.

If we include a weak prior on the Hubble constant, $H_0 > 50$ km s^{-1} Mpc^{-1}, then this is sufficient to constrain $0.98 < \Omega_{\rm tot} < 1.08$ (95% confidence interval). Combining the *WMAP*ext data with supernova measurements of the angular diameter distance relationship (see Fig. 13) we obtain $0.98 < \Omega_{\rm tot} < 1.06$. This confidence interval does not require a prior on h. If we further include the *HST* Key Project measurement of H_0 as a prior, then the limits on Ω_0 improve slightly: $\Omega_{\rm tot} < 1.02 \pm 0.02$. Figure 13 shows the two-dimensional likelihood surface for various combinations of the data.

6.3. *Massive Neutrinos*

Copious numbers of neutrinos were produced in the early universe. If these neutrinos have nonnegligible mass, they can make a nontrivial contribution to the total energy den-

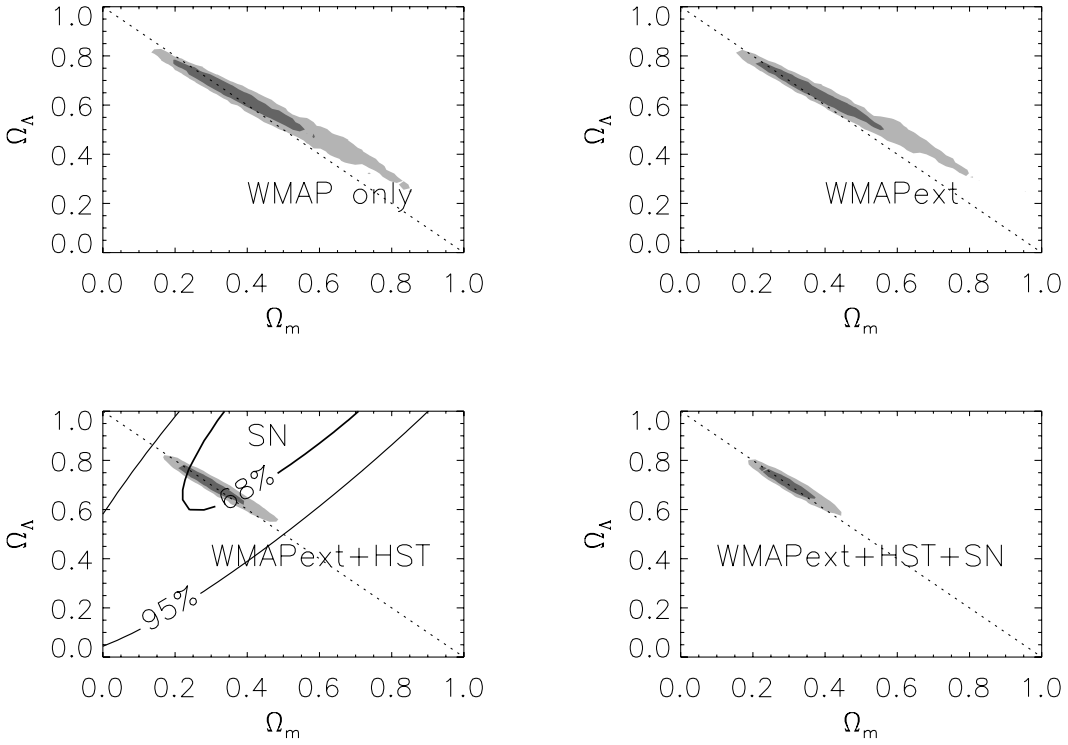

FIG. 13.—Constraints on the geometry of the universe: Ω_m-Ω_Λ plane. Two-dimensional likelihood surface for various combinations of data: *WMAP* (*upper left*); *WMAP*ext (*upper right*); *WMAP*ext+*HST* Key Project (supernova data [Riess et al. 1998, 2001] are shown but not used in the likelihood in this part of the panel) (*lower left*); *WMAP*ext+*HST* Key Project+supernova (*lower right*).

sity of the universe during both matter and radiation domination. During matter domination, the massive neutrinos cluster on very large scales but free-stream out of smaller scale fluctuations. This free-streaming changes the shape of the matter power spectrum (Hu et al. 1998) and, most importantly, suppresses the amplitude of fluctuations. Since we can normalize the amplitude of fluctuations to the *WMAP* data, the amplitude of fluctuations in the 2dFGRS data places significant limits on neutrino properties.

The contribution of neutrinos to the energy density of the universe depends upon the sum of the mass of the light neutrino species:

$$\Omega_\nu h^2 = \frac{\sum_i m_i}{94.0 \text{ eV}} \ . \tag{6}$$

Note that the sum includes only neutrino species light enough to decouple while still relativistic.

Experiments that probe neutrino propagation from source to detector are sensitive not to the neutrino mass but to the square mass difference between different neutrino mass eigenstates. Solar neutrino experiments (Bahcall et al. 2003a) imply that the square mass difference between the electron and muon neutrino is $\sim 10^{-5}$ eV^2. The deficit of muon neutrinos in atmospheric showers imply that the mass difference between muon and tau neutrinos is 10^{-3} eV^2 (Kearns 2002; Pakvasa & Valle 2003). If the electron neutrino is much lighter than the tau neutrino, then the combination of these results imply that $m_{\nu_\tau} < 0.1$ eV: still below the detection limits for our data set. On the other hand, if $m_{\nu_e} \sim m_{\nu_\tau}$, then the three neutrino species can leave an observable imprint on the CMB angular power spectrum and the galaxy large-scale structure power spectrum. In our analysis, we consider this latter case and assume that there are three degenerate stable light neutrino species.

Figure 14 shows the cumulative likelihood of the combination of *WMAP*, CBI, ACBAR, and 2dFGRS data as a function of the energy density in neutrinos. On the basis of this analysis, we conclude that $\Omega_\nu h^2 < 0.0067$ (95% confidence limit). If we add the Lyα data, then the limit slightly weakens to $\Omega_\nu h^2 < 0.0072$. For three degenerate neutrino species, this implies that $m_\nu < 0.23$ eV. This limit is roughly

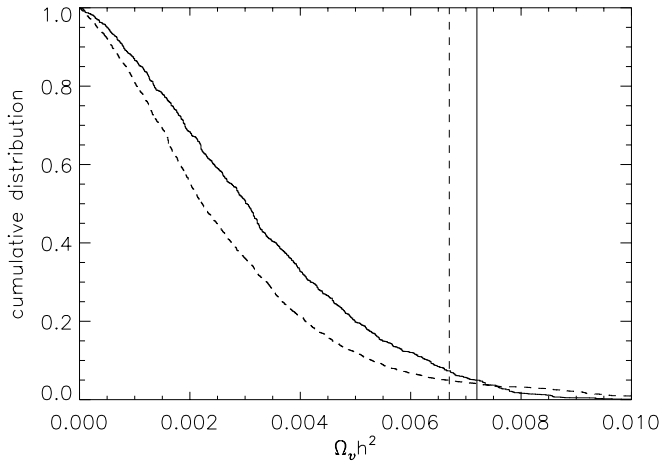

FIG. 14.—Marginalized cumulative probability of $\Omega_\nu h^2$ based on a fit to the *WMAP*ext+2dFGRS data sets (*dashed line*) and the cumulative probability based on a fit to the *WMAP*ext+2dFGRS+Lyα data sets (*solid line*). The vertical lines are the 95% confidence upper limits for each case (0.21 and 0.23 eV).

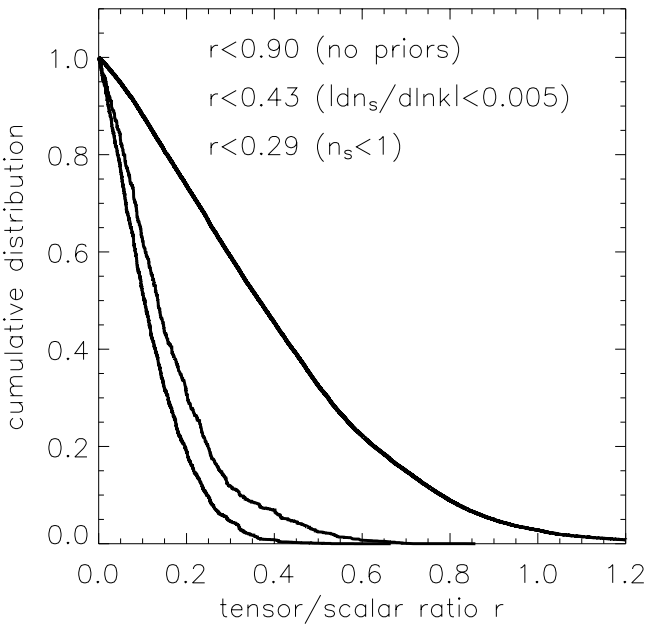

FIG. 15.—Cumulative likelihood of the combination of the *WMAP*ext+2dFGRS+Lyα data sets as a function of r, the tensor/scalar ratio. The three lines show the likelihood for no priors, for models with $|dn/d\ln k| < 0.005$, and for models with $n_s < 1$.

a factor of 2 improvement over previous analyses (e.g., Elgarøy et al. 2002) that had to assume strong priors on Ω_m and H_0.

6.4. *Tensors*

Many models of inflation predict a significant gravity wave background. These tensor fluctuations were generated during inflation. Tensor fluctuations have their largest effects on large angular scales, where they add in quadrature to the fluctuations generated by scalar modes.

Here, we place limits on the amplitude of tensor modes. We define the tensor amplitude using the same convention as Leach et al. (2002):

$$r \equiv \frac{P_{\rm tensor}(k_*)}{P_{\rm scalar}(k_*)} , \tag{7}$$

where $P_{\rm tensor}$ and $P_{\rm scalar}$ are the primordial amplitude of tensor and scalar fluctuations and $k_* = 0.002$ Mpc^{-1}. Since we see no evidence for tensor modes in our fit, we simplify the analysis by assuming that the tensor spectral index satisfies the single field inflationary consistency condition:

$$n_t = -\frac{r}{8} . \tag{8}$$

This constraint reduces the number of parameters in this model to 8: A, $\Omega_b h^2$, $\Omega_m h^2$, h, n_s, $dn_s/d\ln k$, r, and τ. We ignore the running of n_t. The addition of this new parameter does not improve the fit as Figure 15 shows the combination of *WMAP*ext+2dFGRS+Lyα is able to place a limit on the tensor amplitude: $r < 0.90$ (95% confidence limit). As Table 9 shows, this limit is much more stringent if we restrict the parameter space to models with either $n_s < 1$ or $|dn/d\ln k| = 0$.

Peiris et al. (2003) discuss the implications of our limits on tensor amplitude for inflationary scenarios. Using the results of this analysis, Peiris et al. (2003) show that the inferred joint likelihood of n_s, $dn_s/d\ln k$, and r places significant constraints on inflationary models.

7. INTRIGUING DISCREPANCIES

While the ΛCDM model's success in fitting CMB data and a host of other astronomical data is truly remarkable, there remain a pair of intriguing discrepancies: on both the largest and smallest scales. While adding a running spectral index may resolve problems on small scales, there remains a possible discrepancy between predictions and observations on the largest angular scales.

Figure 16 shows the measured angular power spectrum and the predictions of our best-fit ΛCDM model, where the data were fitted to both CMB and large-scale structure data. The figure also shows the measured angular correlation function; the lack of any correlated signal on angular scales greater than 60° is noteworthy. We quantify this lack of power on large scales by measuring a four-point statistic:

$$S = \int_{-1}^{1/2} [C(\theta)]^2 d\cos\theta . \tag{9}$$

The upper cutoff and the form of this statistic were both determined a posteriori in response to the shape of the correlation function. We evaluate the statistical significance of these discrepancies by doing Monte Carlo realizations of the first 100,000 models in the Markov chains. This allows us to average not only over cosmic variance but also over our uncertainties in cosmological parameters. For our ΛCDM Markov chains (fitted to the *WMAP*ext+2dFGRS data sets), we find that only 0.7% of the models have lower values for the quadrupole and only 0.15% of the simulations have lower values of S. For the running model, we find that only 0.9% of the models have lower values for the quadrupole and only 0.3% of the simulations have lower values of S. The shape of the angular correlation function is certainly unusual for realizations of this model.

Is this discrepancy meaningful? The low quadrupole was already clearly seen in *COBE* and was usually dismissed as due to cosmic variance (Bond et al. 1998) or foreground contamination. While the *WMAP* data reinforces the case for its low value, cosmic variance is significant on these large angular scales and any Gaussian field will always have

TABLE 9
95% CONFIDENCE LIMITS ON TENSOR/SCALAR RATIO

Prior	*WMAP*	*WMAP*ext +2dFGRS	*WMAP*ext+2dFGRS+Lyα
None	1.28	1.14	0.90
$dn_s/d\ln k = 0$	0.81	0.53	0.43
$n_s < 1$	0.47	0.37	0.29

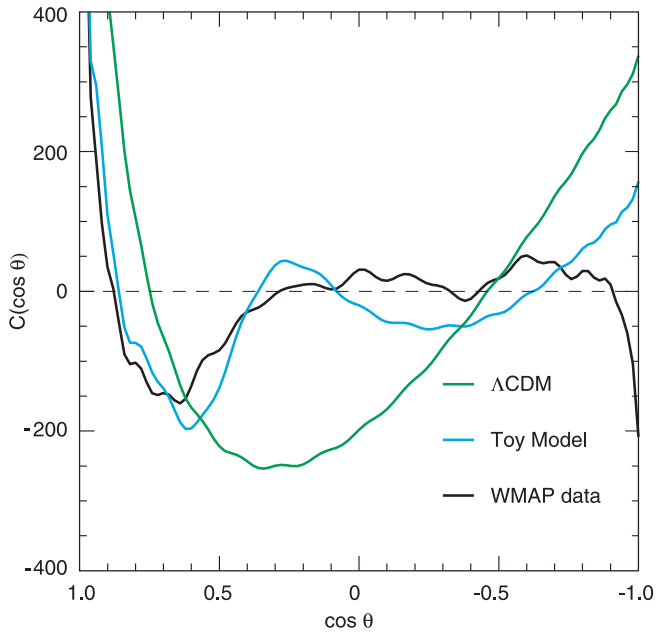

FIG. 16.—Angular correlation function of the best-fit ΛCDM model, toy finite universe model, and *WMAP* data on large angular scales. The data points are computed from the template-cleaned *V*-band *WMAP* using the Kp0 cut (Bennett et al. 2003c).

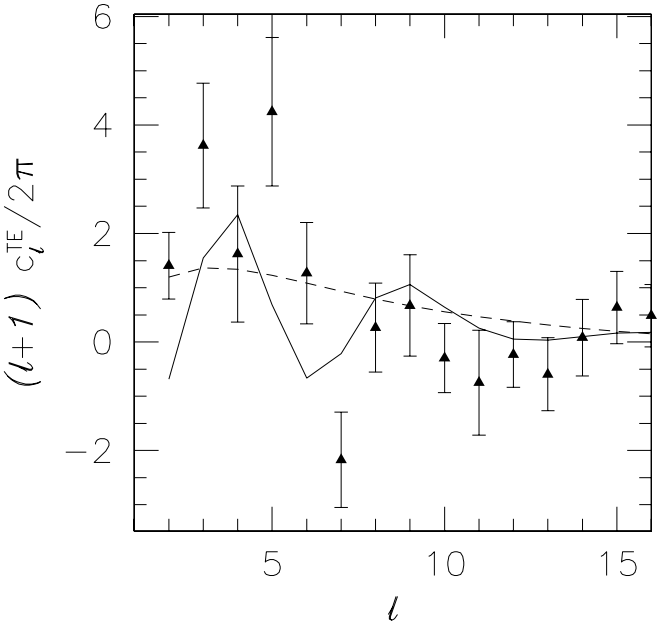

FIG. 17.—TE power spectrum. Comparison of the data to the predicted TE power spectrum in our toy finite universe model and the ΛCDM model. Both models assume that $\tau = 0.17$ and have identical cosmological parameters. This figure shows that the TE power spectrum contains additional information about the fluctuations at large angles. While the current data cannot distinguish between these models, future observations could detect the distinctive TE signature of the model.

unusual features. On the other hand, this discrepancy could be the signature of interesting new physics.

The discovery of an accelerating universe implies that at these large scales, there is new and not understood physics. This new physics is usually interpreted to be dark energy or a cosmological constant. In either case, we would expect that the decay of fluctuations at late times produces a significant ISW signal. Boughn et al. (1998) argue that in a ΛCDM el with $\Omega_m = 0.25$, there should be a detectable correlation between the CMB signal and tracers of large-scale structure; yet they were not able to detect a signal. There are alternative explanations of the accelerating universe, such as extra dimensional gravity theories (Deffayet et al. 2002) that do not require a cosmological constant and should make radically different predictions for the CMB on these angular scales. These predictions have not yet been calculated.

What could generate this unusual shaped angular correlation function? As an example, we compute the angular correlation function in a toy model, where the power spectrum has the form

$$P(k) = \sum_{n=1}^{\infty} \frac{\delta(k - 5.8n/\tau_0)}{k}\ , \qquad (10)$$

where τ_0 is the conformal distance to the surface of last scatter. This toy model simulates both the effects of a discrete power spectrum due to a finite universe and the effects of ringing in the power spectrum due to a feature in the inflaton potential (see Peiris et al. 2003 for a discussion of inflationary models). Figure 16 shows the angular correlation function, and Figure 17 show the TE power spectrum of the model. Note that the TE power spectrum is particularly sensitive to features in the matter power spectrum. Intriguingly, this toy model is a better match to the observed correlation function than the ΛCDM model and predicts a distinctive signature in the TE spectrum. Cornish, Spergel, & Starkman (1998a) show that if the universe was finite and smaller than the volume within the decoupling surface, then there should be a very distinctive signal: matched circles. The surface of last scatter is a sphere centered around *WMAP*. If the universe is finite then this sphere must intersect itself, this leads to pairs of matched circles. These match circles not only provide the definitive signature of a finite universe but also should enable cosmologists to determine the topology of the universe (Cornish et al. 1998b; Weeks 1998). Should we be able to detect circles if the power spectrum cutoff is due to the size of the largest mode being $\sim 1/\tau_0$? While there is no rigorous theorem relating the size of the largest mode to the diameter of the fundamental domain, *D*, analysis of both negatively curved (Cornish & Spergel 2000) and positively curved (Lehoucq et al. 2002) topologies suggest that $D \sim (0.6\text{–}1)\lambda$. Thus, if the "peak" in the power spectrum at $\ell \sim 5$ corresponds to the largest mode in the domain, we should be able to detect a pattern of circles in the sky.

Due to the finite size of the patch of the universe visible to *WMAP* (or any future satellite), our ability to determine the origin and significance of this discrepancy will be limited by cosmic variance. However, future observations can offer some new insight into its origin. By combining the *WMAP* data with tracers of large-scale structure (Boughn et al. 1998; Peiris & Spergel 2000), astronomers may be able to directly detect the component of the CMB fluctuations due to the ISW effect. *WMAP*'s ongoing observations of large-scale microwave background polarization fluctuations will enable additional measurements of fluctuations at large angular scales. Since the TE observations are probing different regions of the sky from the TT observations, they may enlighten us on whether the lack of correlations on large

angular scales is a statistical fluke or the signature of new physics.

8. CONCLUSIONS

Cosmology now has a standard model: a flat universe composed of matter, baryons, and vacuum energy with a nearly scale-invariant spectrum of primordial fluctuations. In this cosmological model, the properties of the universe are characterized by the density of baryons, matter, and the expansion rate: Ω_b, Ω_m, and h. For the analysis of CMB results, all of the effects of star formation can be incorporated in a single number: the optical depth due to reionization, τ. The primordial fluctuations in this model are characterized by a spectral index. Despite its simplicity, it is an adequate fit not only to the *WMAP* temperature and polarization data but also to small-scale CMB data, large-scale structure data, and supernova data. This model is consistent with the baryon/photon ratio inferred from observations of D/H in distant quasars, the *HST* Key Project measurement of the Hubble constant, stellar ages and the amplitude of mass fluctuations inferred from clusters and from gravitational lensing. When we include large-scale structure or Lyα forest data in the analysis, the data suggest that we may need to add an additional parameter: $dn_s/d\ln k$. Since the best-fit models predict that the slope of the power spectrum is redder on small scales, this model predicts later formation times for dwarf galaxies. This modification to the power-law ΛCDM model may resolve many of its problems on the galaxy scale. Table 10 lists the best-fit parameters for this model.

While there have been a host of papers on cosmological parameters, *WMAP* has brought this program to a new stage: *WMAP*'s more accurate determination of the angular power spectrum has significantly reduced parameter uncertainties, *WMAP*'s detection of TE fluctuations has confirmed the basic model and its detection of reionization signature has reduced the n_s-τ degeneracy. Most importantly, the rigorous propagation of errors and uncertainties in the *WMAP* data has strengthened the significance of the inferred parameter values.

In this paper, we have also examined a number of more complicated models: nonflat universes, quintessence models, models with massive neutrinos, and models with tensor gravitational wave modes. By combining the *WMAP* data with finer scale CMB experiments and with other astronomical data sets (2dFGRS galaxy power spectrum and Type Ia supernova observations), we place significant new limits on these parameters.

Cosmology is now in a similar stage in its intellectual development to particle physics three decades ago when particle physicists converged on the current standard model. The standard model of particle physics fits a wide range of data but does not answer many fundamental questions: What is the origin of mass? Why is there more than one family? etc. Similarly, the standard cosmological model has many deep open questions: What is the dark energy? What is the dark matter? What is the physical model behind inflation (or something like inflation)? Over the past three decades, precision tests have confirmed the standard model of particle physics and searched for distinctive signatures of

TABLE 10

Basic and Derived Cosmological Parameters: Running Spectral Index Model

Parameters	Mean and 68% Confidence Errors
Basic	
Amplitude of fluctuations, A	$0.83^{+0.09}_{-0.08}$
Spectral index at $k = 0.05$ Mpc^{-1}, n_s	0.93 ± 0.03
Derivative of spectral index, $dn_s/d\ln k$	$-0.031^{+0.016}_{-0.018}$
Hubble constant, h	$0.71^{+0.04}_{-0.03}$
Baryon density, $\Omega_b h^2$	0.0224 ± 0.0009
Matter density, $\Omega_m h^2$	$0.135^{+0.008}_{-0.009}$
Optical depth, τ	0.17 ± 0.06
Derived	
Matter power spectrum normalization, σ_8	0.84 ± 0.04
Characteristic amplitude of velocity fluctuations, $\sigma_8\Omega_m^{0.6}$	$0.38^{+0.04}_{-0.05}$
Baryon density/critical density, Ω_b	0.044 ± 0.004
Matter density/critical density, Ω_m	0.27 ± 0.04
Age of the universe, t_0	13.7 ± 0.2 Gyr
Reionization redshift,[a] z_r	17 ± 4
Decoupling redshift, $z_{\rm dec}$	1089 ± 1
Age of the universe at decoupling, $t_{\rm dec}$	379^{+8}_{-7} kyr
Thickness of surface of last scatter, $\Delta z_{\rm dec}$	195 ± 2
Thickness of surface of last scatter, $\Delta t_{\rm dec}$	118^{+3}_{-2} kyr
Redshift of matter/radiation equality, $z_{\rm eq}$	3233^{+194}_{-210}
Sound horizon at decoupling, r_s	147 ± 2 Mpc
Angular size distance to the decoupling surface, d_A	$14.0^{+0.2}_{-0.3}$ Gpc
Acoustic angular scale,[b] ℓ_A	301 ± 1
Current density of baryons, n_b	$(2.5 \pm 0.1) \times 10^{-7}$ cm^{-3}
Baryon/photon ratio, η	$(6.1^{+0.3}_{-0.2}) \times 10^{-10}$

Note.—Fit to the *WMAP*, CBI, ACBAR, 2dFGRS, and Lyα forest data.

[a] Assumes ionization fraction, $x_e = 1$.

[b] $l_A = \pi d_C/r_s$.

the natural extension of the standard model: supersymmetry. Over the coming years, improving CMB, large-scale structure, lensing, and supernova data will provide ever more rigorous tests of the cosmological standard model and search for new physics beyond the standard model.

We thank Ed Jenkins for helpful comments about the [D/H] recent measurements and their interpretation. We thank Raul Jimenez for useful discussions about the cosmic ages. We thank Adam Riess for providing us with the likelihood surface form the Type Ia supernova data. The *WMAP* mission is made possible by the support of the Office Space at NASA Headquarters and by the hard and capable work of scores of scientists, engineers, managers, administrative staff, and reviewers. L. V. is supported by NASA through Chandra Fellowship PF2-30022 issued by the *Chandra X-Ray Observatory* center, which is operated by the Smithsonian Astrophysical Observatory for and on behalf of NASA under contract NAS8-39073.

REFERENCES

Bacon, D., Massey, R., Refregier, A., & Ellis, R. 2002, preprint (astro-ph/0203134)
Bahcall, J. N., Gonzalez-Garcia, M. C., & Penya-Garay, C. 2003a, J. High Energy Phys., 2003(02), 009
Bahcall, N. A., & Bode, P. 2002, preprint (astro-ph/0212363)
Bahcall, N. A., Ostriker, J. P., Perlmutter, S., & Steinhardt, P. J. 1999, Science, 284, 1481
Bahcall, N. A., et al. 2002b, preprint (astro-ph/0205490)
Barkana, R., Haiman, Z., & Ostriker, J. P. 2001, ApJ, 558, 482
Barnes, C., et al. 2003, ApJS, 148, 59
Bennett, C. L., et al. 2003a, ApJ, 583, 1
———. 2003b, ApJS, 148, 1
———. 2003c, ApJ, 148, 97
Boesgaard, A. M., & Steigman, G. 1985, ARA&A, 23, 319
Bond, J. R., & Efstathiou, G. 1984, ApJ, 285, L45
Bond, J. R., Jaffe, A. H., & Knox, L. 1998, Phys. Rev. D, 57, 2117
Bond, J. R., et al. 2002, preprint (astro-ph/0205386)
Borgani, S., et al. 2001, ApJ, 561, 13
Boughn, S. P., Crittenden, R. G., & Turok, N. G. 1998, NewA, 3, 275
Brown, M. L., et al. 2002, preprint (astro-ph/0210213)
Burles, S., & Tytler, D. 1998a, ApJ, 499, 699
———. 1998b, ApJ, 507, 732
Burles, S., Nollett, K. M., & Turner, M. S. 2001, ApJ, 552, L1
Caldwell, R. R., Dave, R., & Steinhardt, P. J. 1998, Phys. Rev. Lett., 80, 1582
Carroll, S., Hoffman, M., & Trodden, M. 2003, preprint (astro-ph/0301273)
Cayrel, R., et al. 2001, Nature, 409, 691
Cen, R. 2002, ApJ, submitted (astro-ph/0210473)
Chaboyer, B. 1995, ApJ, 444, L9
———. 1998, Phys. Rep., 307, 23
Chaboyer, B., & Krauss, L. M. 2002, ApJ, 567, L45
Clayton, Donald D. 1988, MNRAS, 234, 1
Colless, M., et al. 2001, MNRAS, 328, 1039
Cornish, N. J., & Spergel, D. N. 2000, Phys. Rev. D, 62, 87304
Cornish, N. J., Spergel, D., & Starkman, G. 1998a, Phys. Rev. D, 57, 5982
———. 1998b, Proc. Natl. Acad. Sci., 95, 82
Cowan, J. J., Pfeiffer, B., Kratz, K.-L., Thielemann, F.-K., Sneden, C., Burles, S., Tytler, D., & Beers, T. C. 1999, ApJ, 521, 194
Croft, R. A. C., Weinberg, D. H., Bolte, M., Burles, S., Hernquist, L., Katz, N., Kirkman, D., & Tytler, D. 2002, ApJ, 581, 20
Croft, R. A. C., Weinberg, D. H., Katz, N., & Hernquist, L. 1998, ApJ, 495, 44
Dedeo, S., Caldwell, R., & Steinhardt, P. 2003, preprint (astro-ph/0301284)
Deffayet, C., Dvali, G., & Gabadadze, G. 2002, Phys. Rev. D, 65, 44023
D'Odorico, S., Dessauges-Zavadsky, M., & Molaro, P. 2001, A&A, 368, L21
Efstathiou, G., & Bond, J. R. 1999, MNRAS, 304, 75
Eke, V. R., Navarro, J. F., & Steinmetz, M. 2001, ApJ, 554, 114
Elgarøy, Ø., et al. 2002, Phys. Rev. Lett., 89, 61301
Epstein, R. I., Lattimer, J. M., & Schramm, D. N. 1976, Nature, 263, 198
Fisher, K. B., Davis, M., Strauss, M. A., Yahil, A., & Huchra, J. 1994, MNRAS, 266, 50
Freedman, W. L., et al. 2001, ApJ, 553, 47
Garnavich, P. M., et al. 1998, ApJ, 509, 74
Gnedin, N. Y., & Hamilton, A. J. S. 2002, MNRAS, 334, 107
Gratton, R. G., Fusi Pecci, F., Carretta, E., Clementini, G., Corsi, C. E., & Lattanzi, M. 1997, ApJ, 491, 749
Haiman, Z., Abel, T., & Rees, M. J. 2000, ApJ, 534, 11
Haiman, Z., Rees, M. J., & Loeb, A. 1997, ApJ, 484, 985
Hannestad, S., Hansen, S. H., Villante, F. L., & Hamilton, A. J. S. 2002, Astropart. Phys., 17, 375
Hansen, B. M. S., et al. 2002, ApJ, 574, L155
Hill, V., et al. 2002, A&A, 387, 560
Hinshaw, G. F., et al. 2003a, ApJS, 148, 135
———. 2003b, ApJS, 148, 63
Hoekstra, H., van Waerbeke, L., Gladders, M. D., Mellier, Y., & Yee, H. K. C. 2002, ApJ, 577, 604
Hu, W. 2001, in Proc. 4th RESCEU Symp., 1999: Birth and Evolution of the Universe, ed. K Sato & M. Kawasaki (Tokyo: Univ. Tokyo Press), 131
Hu, W., Eisenstein, D. J., & Tegmark, M. 1998, Phys. Rev. Lett., 80, 5255
Hu, W., Fukugita, M., Zaldarriaga, M., & Tegmark, M. 2001, ApJ, 549, 669
Huey, G., Wang, L., Dave, R., Caldwell, R. R., & Steinhardt, P. J. 1999, Phys. Rev. D, 59, 63005
Huffenberger, K., & Seljak, U. 2003, preprint (astro-ph/0301341)
Jarosik, N., et al. 2003a, ApJS, 145, 413
———. 2003b, ApJS, 148, 29
Jarvis, M., et al. 2002, preprint (astro-ph/0210604)
Jenkins, E. B., Tripp, T. M., Woźniak, P., Sofia, U. J., & Sonneborn, G. 1999, ApJ, 520, 182
Jimenez, R. 1999, in Dark Matter in Astrophysics and Particle Physics, ed. H. V. Klapdor-Kleingrothaus (Bristol: IOP), 170
Jimenez, R., & Padoan, P. 1998, ApJ, 498, 704
Jimenez, R., Thejll, P., Jorgensen, U. G., MacDonald, J., & Pagel, B. 1996, MNRAS, 282, 926
Jones, M. E., et al. 2001, preprint (astro-ph/0103046)
Kaluzny, J., Thompson, I., Krzeminski, W., Olech, A., Pych, W., & Mochejska, B. 2002, in ASP Conf. Ser. 265, Omega Centauri, a Unique Window into Astrophysics, ed. F. van Leeuwen, J. D. Hughes, & G. Piotto (San Francisco: ASP), 155
Kamionkowski, M., Spergel, D. N., & Sugiyama, N. 1994, ApJ, 426, L57
Kearns, E. T. 2002, Frascati Phys. Ser., 28, 413
Kirkman, D., Tytler, D., Burles, S., Lubin, D., & O'Meara, J. M. 2000, ApJ, 529, 655
Kirkman, D., Tytler, D., Suzuki, N., O'Meara, J., & Lubin, D. 2003, preprint (astro-ph/0302006)
Knox, L., Christensen, N., & Skordis, C. 2001, ApJ, 563, L95
Kogut, A., et al. 2003, ApJS, 148, 161
Komatsu, E., & Seljak, U. 2002, MNRAS, 336, 1256
Komatsu, E., et al. 2003, ApJS, 148, 119
Kosowsky, A., & Turner, M. S. 1995, Phys. Rev. D, 52, 1739
Krauss, L. M., & Chaboyer, B. 2003, Science, 299, 65
Kuo, C. L., et al. 2002, ApJ, submitted (astro-ph/0212289)
Leach, S. M., Liddle, A. R., Martin, J., & Schwarz, D. J. 2002, Phys. Rev. D, 66, 23515
Lehoucq, R., Weeks, J., Uzan, J., Gausmann, E., & Luminet, J. 2002, Classical Quantum Gravity, 19, 4683
Levshakov, S. A., Agafonova, I. I, D'Odorico, S., Wolfe, A. M., & Dessauges-Zavadsky, M. 2003, ApJ, 582, 596
Mason, B. S., Myers, S. T., & Readhead, A. C. S. 2001, ApJ, 555, L11
Moore, B. 1994, Nature, 370, 629
Moos, H. W., et al. 2002, ApJS, 140, 3
Navarro, J. F., Frenk, C. S., & White, S. D. M. 1997, ApJ, 490, 493
Oh, S. P. 2001, ApJ, 553, 499
O'Meara, J. M., Tytler, D., Kirkman, D., Suzuki, N., Prochaska, J. X., Lubin, D., & Wolfe, A. M. 2001, ApJ, 552, 718
Paczyński, B. 1997, in The Extragalactic Distance Scale, ed. M. Livio, M. Donahue, & N. Panagia (Symp. Ser. 10; Baltimore: STScI), 273
Page, L., et al. 2003a, ApJ, submitted
———. 2003b, ApJ, submitted
———. 2003c, ApJ, 585, 566
Pakvasa, S., & Valle, J. W. F. 2003, preprint (hep-ph/0301061)
Peacock, J. A., et al. 2001, Nature, 410, 169
Pearson, T. J., et al. 2002, ApJ, submitted (astro-ph/0205388)
Peebles, P. J. E., & Ratra, B. 1988, ApJ, 325, L17
Peiris, H., et al. 2003, ApJS, 148, 213
Peiris, H. V., & Spergel, D. N. 2000, ApJ, 540, 605
Percival, W. J., et al. 2001, MNRAS, 327, 1297
Perlmutter, S., et al. 1999, ApJ, 517, 565
Pettini, M., & Bowen, D. V. 2001, ApJ, 560, 41
Phillips, M. M. 1993, ApJ, 413, L105
Pierpaoli, E., Borgani, S., Scott, D., & White, M. 2002, preprint (astro-ph/0210567)
Ratra, B., & Peebles, P. J. E. 1988, Phys. Rev. D, 37, 3406

Reese, E. D., Carlstrom, J. E., Joy, M., Mohr, J. J., Grego, L., & Holzapfel, W. L. 2002, ApJ, 581, 53
Refregier, A., Rhodes, J., & Groth, E. J. 2002, ApJ, 572, L131
Reiprich, T. H., & Böhringer, H. 2002, ApJ, 567, 716
Renzini, A., Bragaglia, A., Ferraro, F. R., Gilmozzi, R., Ortolani, S., Holberg, J. B., Liebert, J., Wesemael, F., & Bohlin, R. C. 1996, ApJ, 465, L23
Richer, H. B., et al. 2002, ApJ, 574, L151
Riess, A. G., et al. 1998, AJ, 116, 1009
———. 2001, ApJ, 560, 49
Riess, A. G., Press, W. H., & Kirshner, R. P. 1995, ApJ, 438, L17
Schatz, H., Toenjes, R., Pfeiffer, B., Beers, T. C., Cowan, J. J., Hill, V., & Kratz, K. 2002, ApJ, 579, 626
Schuecker, P., Bohringer,H., Collins, C. A., & Guzzo, L. 2003a, A&A, 398, 867
Schuecker, P., Caldwell, R. R., Bohringer, H., Collins, C. A., Guzzo, L., & Weinberg, N. N. 2003b, A&A, 402, 53
Seljak, U., & Zaldarriaga, M. 1996, ApJ, 469, 437
Sheth, R. K., & Tormen, G. 1999, MNRAS, 308, 119
Sonneborn, G., Tripp, T. M., Ferlet, R., Jenkins, E. B., Sofia, U. J., Vidal-Madjar, A., & Woźniak, P. R. 2000, ApJ, 545, 277
Spergel, D. N., & Steinhardt, P. J. 2000, Phys. Rev. Lett., 84, 3760
Tegmark, M., & Silk, J. 1995, ApJ, 441, 458
Thielemann, F.-K., et al. 2002, Space Sci. Rev., 100, 277
Thompson, I. B., Kaluzny, J., Pych, W., Burley, G., Krzeminski, W., Paczyński, B., Persson, S. E., & Preston, G. W. 2001, AJ, 121, 3089
Toth, G., & Ostriker, J. P. 1992, ApJ, 389, 5
VandenBerg, D. A., Richard, O., Michaud, G., & Richer, J. 2002, ApJ, 571, 487
Van Waerbeke, L., Mellier, Y., Pello, R., Pen, U.-L., McCracken, H. J., & Jain, B. 2002a, A&A, 393, 369
Van Waerbeke, L., Tereno, I., Mellier, Y., & Bernadeau, F. 2002b, preprint (astro-ph/0212150)
Venkatesan, A., Giroux, M. L., & Shull, J. M. 2001, ApJ, 563, 1
Verde, L., et al. 2002, MNRAS, 335, 432
———. 2003, ApJS, 148, 195
Wechsler, R. H., Bullock, J. S., Primack, J. R., Kravtsov, A. V., & Dekel, A. 2002, ApJ, 568, 52
Weeks, J. R. 1998, Classical Quantum Gravity, 15, 2599
Wetterich, C. 1988, Nucl. Phys. B, 302, 668
Willick, J. A., & Strauss, M. A. 1998, ApJ, 507, 64
Zentner, A. R., & Bullock, J. S. 2002, Phys. Rev. D, 66, 43003